Destabilization of a creeping flow by interfacial surfactant: linear theory extended to all wavenumbers

By DAVID HALPERN and ALEXANDER L. FRENKEL

Department of Mathematics, University of Alabama, Tuscaloosa, AL 35487, USA

Creeping flow of a two-layer system with a monolayer of an insoluble surfactant on the interface is considered. The linear-stability theory of plane Couette–Poiseuille flow is developed in the Stokes approximation. To isolate the Marangoni effect, gravity is excluded. The shear-flow instability due to the interfacial surfactant, uncovered earlier for long waves only (Frenkel & Halpern 2002), is studied with inclusion of all wavelengths, and over the entire parameter space of the Marangoni number M, the viscosity ratio m, the interfacial velocity shear s, and the thickness ratio n ($\geqslant 1$). The complex wave speed of normal modes solves a quadratic equation, and the growth rate function is continuous at all wavenumbers and all parameter values. If $M > 0$, $s \neq 0$, $m < n^2$, and $n > 1$, the small disturbances grow provided they are sufficiently long wave. However, the instability is not long wave in the following sense: the unstable waves are not necessarily much longer than the smaller of the two layer thicknesses. On the other hand, there are parametric regimes for which the instability has a mid-wave character, the flow being stable at both sufficiently large and small wavelengths and unstable in between. The critical (instability-onset) manifold in the parameter space is investigated. Also, it is shown that for certain parametric limits the convergence of the dispersion function is non-uniform with respect to the wavenumber. This is used to explain the parametric discontinuities of the long-wave growth-rate exponents found earlier.

1. Introduction

There has been considerable interest in the instability of two-layer flows as well as in the influence of surfactants, since they occur in many industrial and biomedical applications such as oil recovery (e.g. Slattery 1974), lubricated pipelining (e.g. Joseph & Renardy 1993), coating in photography (e.g. Kistler & Schweizer 1997), and the obstruction to airflow in the small airways of the lungs (e.g. Halpern & Grotberg 1993; Otis *et al.* 1993).

Yih (1967) discovered an instability of a plane Couette–Poiseuille flow of two fluid layers with different viscosities and densities by considering long waves in the linear theory. The study of this instability was extended to shorter waves and different parametric conditions by many researchers. An overview and summary of this work was given by Joseph & Renardy (1993) and, more recently, by Charru & Hinch (2000). The Yih instability is due to inertia effects, which will play no role in the present paper.

Another well-studied two-fluid system is the core–annular flow (CAF), a layered arrangement of two immiscible fluids that fill a circular pipe and flow along its axis.

Examples of such flows include separated flow of steam and water in power generation facilities and lubricated pipelining of crude viscous oils (e.g. Joseph & Renardy 1993). These types of flows are also found in the lungs where air passes through airways lined with a viscous liquid layer. Closure of the small airways of the lungs may occur as a result of a surface-tension-driven instability. This type of capillary instability often happens in premature neonates who do not produce sufficient quantities of surfactant that tends to keep the surface tension low and is vital for healthy, normal breathing. It has been shown that the presence of surfactant can delay and potentially prevent the capillary instability (Halpern & Grotberg 1993; Otis *et al.* 1993). Linear stability theory for a thin stagnant film shows that in the limit of an immobilized insoluble surfactant monolayer, the instability growth rate is reduced by a factor of four compared to the clean surface case (Carroll & Lucassen 1974; Cassidy *et al.* 1999). Recently (in an unpublished work), H. Wei & D. Rumschitzki considered the combined effects of the basic core–annular flow, capillarity and surfactant. For small Marangoni numbers, they found that the coupling between surfactants and the base core–annular flow could enhance the capillary instability: the maximum growth rate increases somewhat and the range of unstable wavenumbers expands.

In general, the effect of introducing insoluble surfactants (without changing the base flow) always appeared in the literature to be stabilizing or neutral. Our recent work (Frenkel & Halpern 2002) suggests that this is due to the fact that in those earlier cases the interfacial velocity shear was zero. This was the case because the surfactant systems studied there were either single-fluid flows with a free surface (Whitaker 1964; Whitaker & Jones 1966; Yih 1966; Anshus & Acrivos 1967; Lin 1970; De Wit, Gallez & Christov 1994; Rubinstein & Bankoff 2001) or multifluid systems with no base flow (Kwak & Pozrikidis 2001). Two-fluid systems combining the imposed basic flow with interfacial surfactant were not studied until recently. In Frenkel & Halpern (2002), we showed that the simultaneous presence of the surfactant and velocity shear at the interface is sufficient for the instability (in a certain range of parameters) of the basic flow. We believe that it was the first example of a system stable in the absence of surfactants but destabilized by the introduction of an interfacial surfactant (such that the basic flow remains intact). Also, it provided the first example of the destabilization of a stagnant two-fluid system by the imposition of a Stokes flow. The instabilities of other, surfactant-less two-layer wall-bounded Stokes flows – due to such factors as gravity (Babchin *et al.* 1983*b*; Halpern & Frenkel 2001), molecular van der Waals forces (Babchin *et al.* 1983*a*), capillarity (Frenkel *et al.* 1987; Hu & Joseph 1989), buoyancy (Gumerman & Homsy 1974) – can be seen to have the same growth rates as in the stagnant case, so for those cases the basic flow is irrelevant to the linear instability (although important for the nonlinear saturation of the instability).

However, in Frenkel & Halpern (2002) we considered only *long-wave* behaviour of the surfactant instability (of the two-layer Couette–Poiseuille flow between two parallel plates). In the present work, we extend the study to include all wavenumbers. It turns out that this Stokes-flow instability lends itself to a rather complete characterization. Some questions left unanswered in the long-wave theory are resolved here.

In §2, the governing equations for the system in question are laid out. The linear-stability analysis using normal modes with arbitrary wavenumbers is presented in §3. Results are given in §4, and some concluding remarks are given in §5.

2. Governing equations

The exact formulation of the problem (as given earlier in Frenkel & Halpern 2002) is as follows. Consider two immiscible fluid layers between two infinite parallel
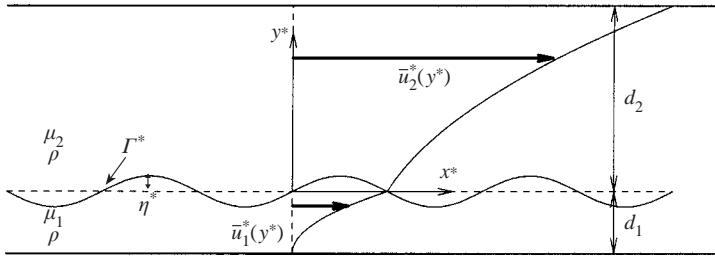
FIGURE 1. Definition sketch for a two-layer Couette–Poiseuille flow between a fixed plate at $y^* = -d_1$ and a moving plate at $y^* = d_2$. The disturbed interface $y^* = \eta^*(x^*, t^*)$ is shown as a sinusoidal solid curve. $\Gamma^*(x^*, t^*)$ is the concentration of the insoluble surfactant monolayer. The solid curve spanning the flow is the profile of the basic velocity (bold arrows). (If the pressure gradient is turned off, the velocity profile becomes piecewise-linear: the Couette flow.)

plates, as in figure 1 (see also figure 1 of Yih 1967). Let the basic flow be driven by the combined action of an in-plane steady motion of one of the plates and a constant pressure gradient parallel to the plate velocity and directed in the same or opposite sense. It is well known that the basic 'Couette–Poiseuille' velocity profiles are steady and vary (quadratically) in the spanwise direction only, and the basic interface between the fluids is flat. For simplicity, let the densities of the two fluids be equal. Then gravity does not affect the stability of the basic flow, and is disregarded below. It is convenient to use the reference frame of the unperturbed interface. Let y^* be the spanwise, 'vertical', coordinate (the symbol * indicates a dimensional quantity). Let the interface be at $y^* = 0$ and the y^*-axis directed from the thinner layer to the thicker one; we will call this the 'upward' direction (clearly, since there is no gravity, the notions of 'up' and 'down' are a matter of convention). Thus, $d_1 < d_2$ holds, where d_1 and d_2 are the thicknesses of the lower and upper fluids, respectively. The direction of the 'horizontal' x^*-axis is chosen so that velocity of the lower plate, located at $y^* = -d_1$, is $-U_1$ if U_1 is the relative speed of the interface and the lower plate. The velocity U_2 of the upper plate (situated at $y^* = d_2$) is positive for the purely Couette flow; however, it does not have to be positive in the presence of a pressure gradient. For the Couette flow, in which the velocity profiles are linear, it is easy to see that, in terms of U, the velocity of the upper plate relative to the lower plate (i.e. $U = U_1 + U_2$), we have $U_1 = \mu_2 d_1 (\mu_2 d_1 + \mu_1 d_2)^{-1} U$ and $U_2 = \mu_1 d_2 (\mu_2 d_1 + \mu_1 d_2)^{-1} U$, where μ_1 and μ_2 are the viscosities of the lower and upper fluids, respectively. For the more general (quadratic) Couette–Poiseuille flow, it is also not difficult to express U_1 and U_2 in terms of the two 'physical' quantities U and the basic pressure gradient; however, we will not need these expressions.

The well-known Squire's theorem (proved for our case in Appendix C; also see Hesla, Prankch & Preziosi 1986; Joseph & Renardy 1993) allows us to confine our consideration to two-dimensional perturbed flows (in the $x^* y^*$-plane). The equation of the perturbed interface is $y^* = \eta^*(x^*, t^*)$, and the Navier–Stokes and incompressibility equations governing the fluid motion in the two layers are (with $j = 1$ for the lower layer and $j = 2$ for the upper one)

$$\rho \left(\frac{\partial \boldsymbol{v}_j^*}{\partial t^*} + \boldsymbol{v}_j^* \cdot \boldsymbol{\nabla}^* \boldsymbol{v}_j^* \right) = -\boldsymbol{\nabla}^* p_j^* + \mu_j \boldsymbol{\nabla}^{*2} \boldsymbol{v}_j^*, \quad \boldsymbol{\nabla}^* \cdot \boldsymbol{v}_j^* = 0, \tag{2.1}$$

where $\boldsymbol{\nabla}^* = (\partial/\partial x^* / \partial/\partial y^*)$, ρ is the density (of both fluids), $\boldsymbol{v}_j^* = (u_j^*, v_j^*)$ is the fluid

velocity with horizontal component u_j^* and vertical component v_j^*, and p_j^* is the pressure.

We use the 'no-slip, no-penetration' boundary conditions (requiring zero relative velocities) at the plates: $u_1^* = -U_1$, $v_1^* = 0$ at $y^* = -d_1$; and $u_2^* = U_2$, $v_2^* = 0$ at $y^* = d_2$. The interfacial boundary conditions are as follows. The velocity must be continuous at the interface: $[\boldsymbol{v}^*]_1^2 = 0$, where $[A]_1^2 = A_2 - A_1$ denotes the jump in A across the interface, i.e. at $y^* = \eta^*(x^*, t^*)$. The interfacial balances of the tangential and normal stresses, taking into account the jump in the tangential stress due to the variability of surface tension and the capillary jump in the normal stress, are

$$\frac{1}{1+\eta_{x^*}^{*2}}\left[(1-\eta_{x^*}^{*2})\mu(u_{y^*}^* + v_{x^*}^*) + 2\eta_{x^*}^{*2}\mu(v_{y^*}^* - u_{x^*}^*)\right]_1^2 = -\frac{\sigma_{x^*}^*}{\left(1+\eta_{x^*}^{*2}\right)^{1/2}}, \qquad (2.2)$$

$$\left[(1+\eta_{x^*}^{*2})p^* - 2\mu\left(\eta_{x^*}^{*2}u_{x^*}^* - \eta_{x^*}^*(u_{y^*}^* + v_{x^*}^*) + v_{y^*}^*\right)\right]_1^2 = \frac{\eta_{x^*x^*}^*}{\left(1+\eta_{x^*}^{*2}\right)^{1/2}}\sigma^*, \qquad (2.3)$$

where σ^* is the surface tension. The kinematic interfacial condition is $\eta_{t^*}^* = v^* - u^*\eta_{x^*}^*$. The surface concentration of the insoluble surfactant on the interface, $\Gamma^*(x^*, t^*)$, obeys the following equation (see a simple derivation in Appendix B):

$$\frac{\partial(H\Gamma^*)}{\partial t^*} + \frac{\partial}{\partial x^*}(H\Gamma^* u^*) = D_s \frac{\partial}{\partial x^*}\left(\frac{1}{H}\frac{\partial\Gamma^*}{\partial x^*}\right), \qquad (2.4)$$

where $H = \sqrt{1 + \eta_x^{*2}}$, and D_s is the surface molecular diffusivity of surfactant; D_s is usually negligible, and is discarded below. (This equation can be obtained from the two-dimensional one derived by Wong, Rumschitzki & Maldarelli (1996) and, independently, by Li & Pozrikidis (1997) (and written there in general moving curvilinear coordinates); however, showing this appears to be harder than directly deriving equation (2.4) from first principles, as in Appendix B, by using only fixed Cartesian coordinates (those entering equation (2.4)).) Since we only deal with infinitesimal deviations of the concentration $\Gamma^*(x^*, t^*)$ from its basic value Γ_0, we can linearize the surface tension dependence on the surfactant concentration: $\sigma^* = \sigma_0 - E(\Gamma^* - \Gamma_0)$, where σ_0 is the basic surface tension and E is a constant.

We introduce dimensionless variables as follows:

$$(x, y) = \frac{(x^*, y^*)}{d_1}, \quad t = \frac{t^*}{d_1\mu_1/\sigma_0}, \quad (u, v) = \frac{(u^*, v^*)}{\sigma_0/\mu_1}, \quad p = \frac{p^*}{\sigma_0/d_1}, \quad \Gamma = \frac{\Gamma^*}{\Gamma_0}, \quad \sigma = \frac{\sigma^*}{\sigma_0}. \qquad (2.5)$$

The dimensionless velocity field of the basic Couette–Poiseuille flow, with a flat interface, $\eta = 0$, and uniform concentration of surfactant, $\bar{\Gamma} = 1$ (where the overbar indicates a basic-state quantity), is

$$\bar{u}_1(y) = sy + qy^2, \quad \bar{v}_1 = 0 \quad \text{for} -1 \leqslant y \leqslant 0, \qquad (2.6)$$

$$\bar{u}_2(y) = \bar{u}_1(y)/m, \quad \bar{v}_2 = 0 \quad \text{for } 0 \leqslant y \leqslant n, \qquad (2.7)$$

where $1 \leqslant n = d_2/d_1$ and $m = \mu_2/\mu_1$. The constants s and q will be used in place of the pressure gradient and the relative velocity of the plates to characterize the basic flow. As will be seen below, the stability depends only on the 'shear' coefficient s (and not on q), the interfacial slope of the profile $\bar{u}_1(y)$ of the basic film velocity: $s = \mathrm{d}\bar{u}_1(0)/\mathrm{d}y$.

3. Stability problem formulation

The formulation of the linear problem for infinitesimal disturbances is the same as in Frenkel & Halpern (2002) up to the Stokes equations (3.11) below. Beyond that point, the analyses are different.

We consider the perturbed state with small deviations from the basic flow: $\eta = \tilde{\eta}$, $u_j = \bar{u}_j + \tilde{u}_j$, $v_j = \tilde{v}_j$, $p_j = \tilde{p}_j$ and $\Gamma = 1 + \tilde{\Gamma}$ (with $\bar{u}_j$ given in equations (2.6) and (2.7)). It is convenient to introduce disturbance stream functions $\tilde{\psi}_j$ such that $\tilde{u}_j = \tilde{\psi}_{jy}$, and $\tilde{v}_j = -\tilde{\psi}_{jx}$. We use normal modes

$$(\tilde{\eta}, \tilde{\psi}_j, \tilde{p}_j, \tilde{\Gamma}) = [h, \phi_j(y), f_j(y), g]e^{i\alpha(x-ct)}, \tag{3.1}$$

where α is the wavenumber of the disturbance, g and h are constants and $c = c_R + ic_I$ is the complex wave speed. The growth rate γ depends on the imaginary part of c only: $\gamma = \alpha c_I$. Linearizing the kinematic boundary condition yields $\tilde{\eta}_t(x, t) = -\tilde{\psi}_x(x, 0, t)$. Hence h is expressed in terms of the stream function:

$$h = \phi_1(0)/c \tag{3.2}$$

(assuming $c \neq 0$). The linearization of the horizontal and vertical components of the momentum equations (2.1) yields ($j = 1, 2$)

$$m_j D(D^2 - \alpha^2)\phi_j - i\alpha f_j = i\alpha \frac{Re}{Ca}[(\bar{u}_j - c)D\phi_j - \phi_j D\bar{u}_j], \tag{3.3}$$

$$i\alpha m_j(D^2 - \alpha^2)\phi_j + Df_j = -\alpha^2 \frac{Re}{Ca}(\bar{u}_j - c)\phi_j \tag{3.4}$$

where $m_1 = 1$, $m_2 = m$, $D = d/dy$, $Re = \rho U_1 d_1/\mu_1$, the Reynolds number, and $Ca = \mu_1 U_1/\sigma_0$, the capillary number. Eliminating the pressure disturbances f_j from equations (3.3) and (3.4), we obtain the well-known Orr–Sommerfeld equations for the stream-functions:

$$m_j(D^2 - \alpha^2)^2\phi_j = i\alpha \frac{Re}{Ca}[(\bar{u}_j - c)(D^2 - \alpha^2)\phi_j - \phi_j D^2\bar{u}_j]. \tag{3.5}$$

The disturbance stream functions ϕ_j are subject to the boundary conditions at the plates and at the interface. The boundary conditions at the plates require

$$\phi_1(-1) = \phi_1'(-1) = \phi_2(n) = \phi_2'(n) = 0, \tag{3.6}$$

where we use a prime to indicate differentiation with respect to y. Continuity of velocity at the interface implies

$$\phi_1(0) = \phi_2(0) \tag{3.7}$$

and

$$m(\phi_1'(0) - \phi_2'(0)) = (1 - m)\frac{s}{c}\phi_1(0). \tag{3.8}$$

After linearization, the normal stress condition, equation (2.3), yields

$$m\phi_2'''(0) - \phi_1'''(0) - 3\alpha^2[m\phi_2'(0) - \phi_1'(0)] = -i\frac{\alpha^3}{c}\phi_2(0). \tag{3.9}$$

The linearized tangential stress condition, equation (2.2), is $m\phi_2''(0) - \phi_1''(0) + \alpha^2(m\phi_2(0) - \phi_1(0)) = iM\alpha g$, where $M = E\Gamma_0/\sigma_0$ is the Marangoni number. We replace the constant g in this equation by its expression from the linearized surfactant transport equation (derived from (2.4)), $\tilde{\Gamma}_t + \bar{u}_{1y}(0)\tilde{\eta}_x + \tilde{\psi}_{1xy}(x, 0, t) = 0$, whence $g = \phi_1'(0)/c + s\phi_1(0)/c^2$. As a result, the linearized tangential-stress balance condition

is written purely in terms of stream functions:

$$m\phi_2''(0) - \phi_1''(0) + \alpha^2[m\phi_2(0) - \phi_1(0)] = iM\frac{\alpha}{c}\left[\phi_1'(0) + \frac{s}{c}\phi_1(0)\right]. \quad (3.10)$$

For each α, the linear (in ϕ_j) equations (3.5)–(3.10) constitute an eigenvalue problem determining the (complex) phase velocity c. In the limit of Stokes flow, equations (3.3) and (3.4) reduce to

$$(D^2 - \alpha^2)^2\phi_j = 0. \quad (3.11)$$

In Frenkel & Halpern (2002), we considered the long-wave ($\alpha \to 0$) simplification, $D^4\phi_j = 0$, with general solutions $\phi_j(y) = A_j + B_jy + C_jy^2 + D_jy^3$. Here, we study the full equations (3.11), with general solutions

$$\phi_j(y) = A_j \cosh\alpha y + B_j \sinh\alpha y + C_jy \cosh\alpha y + D_jy \sinh\alpha y, \quad (3.12)$$

where the coefficients A_j, B_j, C_j and D_j are determined by the boundary conditions up to a common normalization factor. (We note that these coefficients can depend on α, etc., and even be unbounded as $\alpha \to 0$, as in table 1 of Frenkel & Halpern 2002.) We choose the normalization $A_1 = 1$, then also $A_2 = 1$, so that $\phi_1(0) = 1 = \phi_2(0)$ (see equation (3.7)).

By applying the plate velocity conditions (3.6), and the continuity of tangential velocity, (3.8), the coefficients C_1 and D_1 can be expressed in terms of B_1, and C_2 and D_2 in terms of B_2, so that

$$\phi_1(y) = \cosh(\alpha y) + B_1 \sinh(\alpha y) + \left[-\frac{s_\alpha^2}{\alpha}B_1 + 1 + \frac{s_\alpha c_\alpha}{\alpha}\right]y\cosh(\alpha y)$$
$$+ \left[\left(1 - \frac{s_\alpha c_\alpha}{\alpha}\right)B_1 + \frac{c_\alpha^2}{\alpha}\right]y\sinh(\alpha y) \quad (3.13)$$

and

$$\phi_2(y) = \cosh(\alpha y) + B_2 \sinh(\alpha y) - \left[\frac{s_{\alpha n}^2}{\alpha n^2}B_2 + \frac{1}{n} + \frac{s_{\alpha n}c_{\alpha n}}{\alpha n^2}\right]y\cosh(\alpha y)$$
$$+ \left[\left(-\frac{1}{n} + \frac{s_{\alpha n}c_{\alpha n}}{\alpha n^2}\right)B_2 + \frac{c_{\alpha n}^2}{\alpha n^2}\right]y\sinh(\alpha y), \quad (3.14)$$

where

$$c_\alpha = \cosh(\alpha), \quad s_\alpha = \sinh(\alpha), \quad c_{\alpha n} = \cosh(\alpha n), \quad s_{\alpha n} = \sinh(\alpha n). \quad (3.15)$$

The interfacial conditions (3.8)–(3.10) then provide the following three equations involving B_1, B_2 and c:

$$\left(\alpha - \frac{s_\alpha^2}{\alpha}\right)B_1 + \left(\frac{s_{\alpha n}^2}{\alpha n^2} - \alpha\right)B_2 + \frac{n+1}{n} + \frac{1}{\alpha}\left(s_\alpha c_\alpha + \frac{s_{\alpha n}c_{\alpha n}}{n^2}\right) + \left(1 - \frac{1}{m}\right)\frac{s}{c} = 0, \quad (3.16)$$

$$2mB_2 - 2B_1 - \frac{i}{c} = 0, \quad (3.17)$$

and

$$\left[\frac{iM}{c}(s_\alpha^2 - \alpha^2) - 2(\alpha - c_\alpha s_\alpha)\right]B_1 - \frac{2\alpha m}{n}\left(1 - \frac{s_{\alpha n}c_{\alpha n}}{\alpha n}\right)B_2 + 2\frac{m}{n^2}c_{\alpha n}^2 - 2c_\alpha^2$$
$$- 2\alpha^2(1 - m) - \frac{i\alpha M}{c}\left(1 + \frac{s}{c} + \frac{s_\alpha c_\alpha}{\alpha}\right) = 0. \quad (3.18)$$

Solving equation (3.17) yields B_2 in terms of B_1. This expression is substituted into (3.16) which then yields B_1, and thus B_2, in terms of c. Substituting these expressions for B_1 and B_2 in terms of c into (3.18), we obtain a quadratic equation for the phase velocity:

$$q_2 c^2 + q_1 c + q_0 = 0, \tag{3.19}$$

where the coefficients q_0, q_1 and q_2 are given by

$$q_0 = \frac{1}{4} \frac{M}{\alpha} \left(\alpha^2 n^2 - s_{\alpha n}^2 \right) \left(\alpha^2 - s_\alpha^2 \right) - \frac{i}{2} M s \left(s_{\alpha n}^2 - s_\alpha^2 n^2 \right), \tag{3.20}$$

$$
\begin{aligned}
q_1 = {}& (m-1) s (\alpha n^2 - n^2 s_\alpha c_\alpha + \alpha n - s_{\alpha n} c_{\alpha n}) \\
& + \frac{i}{2} \Bigg[(\alpha n + s_{\alpha n} c_{\alpha n}) \left(\alpha - \frac{s_\alpha^2}{\alpha} \right) m M + \left(\alpha^2 n^2 - s_{\alpha n}^2 \right) \left(1 + \frac{s_\alpha c_\alpha}{\alpha} \right) M \\
& - (\alpha n - s_{\alpha n} c_{\alpha n}) \left(\alpha - \frac{s_\alpha^2}{\alpha} \right) m - \left(\alpha^2 n^2 - s_{\alpha n}^2 \right) \left(1 - \frac{s_\alpha c_\alpha}{\alpha} \right) \Bigg],
\end{aligned}
\tag{3.21}
$$

$$
\begin{aligned}
q_2 = {}& \left(\alpha - \frac{s_\alpha^2}{\alpha} \right) \left(\alpha^2 n^2 + c_{\alpha n}^2 \right) m^2 + 2 \left(\alpha n - \alpha^3 n^2 - \frac{s_\alpha c_\alpha s_{\alpha n} c_{\alpha n}}{\alpha} \right) m \\
& + \left(\alpha + \frac{c_\alpha^2}{\alpha} \right) \left(\alpha^2 n^2 - s_{\alpha n}^2 \right). \tag{3.22}
\end{aligned}
$$

Using the well-known formula for solving the quadratic equation, c is an elementary function of α and the parameters. We are interested in the dependence of the growth rate $\gamma = \alpha c_I$ on the wavenumber α and the parameters M, s, m and n. The solution of equation (3.19) shows that the dependence of the growth rate on s is even: $\gamma(-s) = \gamma(s)$. We will consider the growth rate for the parameter ranges $0 \leqslant M, s, m < \infty \, (m > 0)$ and $1 \leqslant n \leqslant \infty$.

4. Characterization of instability

4.1. *Broad overview*

In Frenkel & Halpern (2002), we considered only the long-wave disturbances, which was sufficient to establish the existence of the instability. We showed that, provided the shear s was non-zero, the system was linearly unstable for $m < n^2$ and stable for $m \geqslant n^2$. This did not exclude the possibility of instability for $m \geqslant n^2$ with respect to shorter-wave disturbances. Our present analysis covering all wavelengths will show this possibility to exist.

There are always two normal modes. If one of them is growing with time (the growth rate is positive, see figure 2a) for a certain interval of wavenumbers α, the other one decays (see figure 2b) for all α. For the growing mode, the 'dispersion curve' $\gamma = \gamma(\alpha)$ (at any values of the 'control parameters' M, m, s, and n) starts from the zero value at $\alpha = 0$. It reaches a maximum $\gamma_{\max}$ at some $\alpha = \alpha_{\max}$, then falls monotonically, passing from positive to negative values at some 'marginal wavenumber' α_0. (This typical behaviour is illustrated in figure 2(a) for a few representative choices of parameters.) Thus the ('longer-wave') interval of wavenumbers of disturbances to which the system is unstable is $0 \leqslant \alpha_1 < \alpha < \alpha_0$. All the quantities $\gamma_{\max}$, $\alpha_{\max}$, α_1 and α_0 depend on the control parameters M, m, s and n.

The instability threshold $m \leqslant n^2$ applies if $M < 5/2$. For $M > 5/2$, there are growing modes for a finite (and depending on the other parameters) interval of $m > n^2$. The
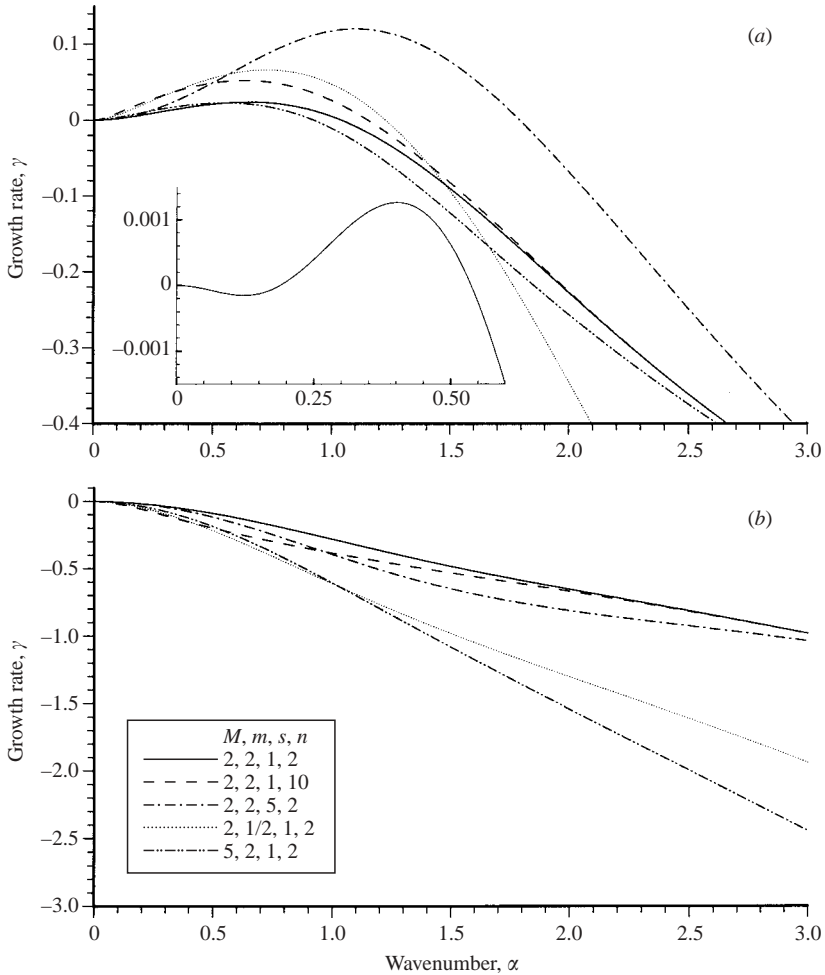
FIGURE 2. Dispersion curves (growth rate versus the wavenumber) of (*a*) the unstable mode and (*b*) the stable mode for a few sample values of the parameters. For the inset, $n = 4$, $M = 5$, $s = 1$ and $m = 17$.

corresponding dispersion curves have positive growth rates for a finite α-interval bounded away from $\alpha = 0$ (which situation we call the 'mid-wave' instability, as opposed to the long-wave and short-wave ones). An example of such dispersion curve is shown in figure 2(*a*) (see the inset).

In all cases we considered, the ratio α_0 / α_{max} is of magnitude-order 1, as illustrated by table 1. (However, it can be large for unrealistically large values of s; see Appendix D.) Moreover, γ_{max} has a (single) maximum as a function of the Marangoni number M at fixed values of m, n and s as is illustrated by figure 3(*a*) for some representative parameter values. (In fact, our computations suggest that $\gamma_{max} \to 0$ as $M \to \infty$, the limit in which the surface is immobilized by the surfactant.) Thus, γ has a maximum γ_M at some point in the plane of α and M, as is seen in figure 4 which displays level curves of $\gamma(\alpha, M)$ in the (α, M)-plane. We call the coordinates of the point of this maximum α_M and M_M (so that $\gamma(\alpha_M, M_M) = \gamma_M$).

$\dfrac{\alpha_0}{\alpha_{\max}}(M=V)$	$\dfrac{\alpha_0}{\alpha_{\max}}(s=V)$	$\dfrac{\alpha_0}{\alpha_{\max}}(m=V)$	$\dfrac{\alpha_0}{\alpha_{\max}}(n-1=V)$
V	$(m=2,\,n=2,\,s=1)$	$(M=1,\,m=2,\,n=2)$	$(M=1,\,n=20,\,s=1)$	$(M=1,\,m=1/2,\,s=1)$
$\frac{1}{100}$	1.415	1.953	1.748	1.343
1	1.561	1.561	1.814	1.662
100	2.773	1.486	1.474	1.788

TABLE 1. Ratio $\alpha_0/\alpha_{\max}$ for a wide range of sample parameter values: Each of M, s, m and $n-1$ takes the three values $V=0.01,1,100$, with the other three parameters being fixed as shown at the top of the corresponding column.

Each of the quantities γ_M, α_M and M_M is a function of the three variables m, s and n. Each of these functions can be visualized by their level surfaces in the three-dimensional parameter space with (Cartesian) coordinates m, s and n.

Figures 5 to 7 show the level curves which are cross-sections of such level surfaces through the $n=$ const planes at four representative values of n, namely $n=1.1$, 2, 11 and ∞. In addition, figure 8 is a plot of the same type for the phase velocity c_R. These figures give a broad view of the parametric behaviour of the instability. [Note that for the case of an infinitely thick layer, $n=\infty$, the eigenfunctions of the form (3.12) do not apply. Instead the appropriate eigenfunction for the upper layer is $\phi_2(y)=\mathrm{e}^{-\alpha y}(1+yB_2)$. The same steps as in §3 lead to somewhat different coefficients of the quadratic equation (3.19) for the phase velocity:

$$q_0 = -\frac{1}{4}\frac{M}{\alpha}\left(\alpha^2-s_\alpha^2\right)-\frac{\mathrm{i}}{2}Ms, \tag{4.1}$$

$$q_1 = (1-m)s + \frac{\mathrm{i}}{2}\left[\left(\alpha-\frac{s_\alpha^2}{\alpha}\right)mM - \left(1+\frac{s_\alpha c_\alpha}{\alpha}\right)M + \left(\alpha-\frac{s_\alpha^2}{\alpha}\right)m + \left(1-\frac{s_\alpha c_\alpha}{\alpha}\right)\right], \tag{4.2}$$

and

$$q_2 = \left(\alpha-\frac{s_\alpha^2}{\alpha}\right)m^2 - 2\frac{s_\alpha c_\alpha}{\alpha}m - \left(\alpha+\frac{c_\alpha^2}{\alpha}\right). \tag{4.3}$$

The same expressions are obtained by multiplying the general coefficients (3.20)–(3.22) by $\mathrm{e}^{-2\alpha n}$ and taking the limit $n\to\infty$.]

The behaviour of γ_M (figure 5) is the subject of the next subsection. As regards other characteristic quantities, we notice the following. It appears from figure 6 that α_M is larger where m is smaller, s is larger, and n is larger, with α_M already being close to its $n=\infty$ asymptotics at $n=11$. Figure 7 shows that M_M also almost reaches its $n=\infty$ asymptotics at $n=11$, increasing with m and s. However, at smaller n, the dependence on m is non-monotonic, having the minimum at m of magnitude-order one, where the system is close to the stability boundary $m=n^2$. A similar non-monotonicity appears in figure 8 for the wave speed c_{MR}.

For the other two characteristic quantities, $\alpha_{\max}$ and α_0, which are plotted in figure 3 for a few representative points of the parameter space, we find that, for $m>1$, each of them attains a single maximum at some $M\neq0$, similar to that of $\gamma_{\max}(M)$, and approaches zero as $M\to0$. However, for $m<1$, the functions $\alpha_{\max}(M)$ and $\alpha_0(M)$ may attain no such maxima, and they do not vanish as $M\to0$. (See the curves for $m=1/2$ in figure 3.) Instead, they tend to finite limits $\alpha_{\max0}$ and α_{00} as $M\to0$. We

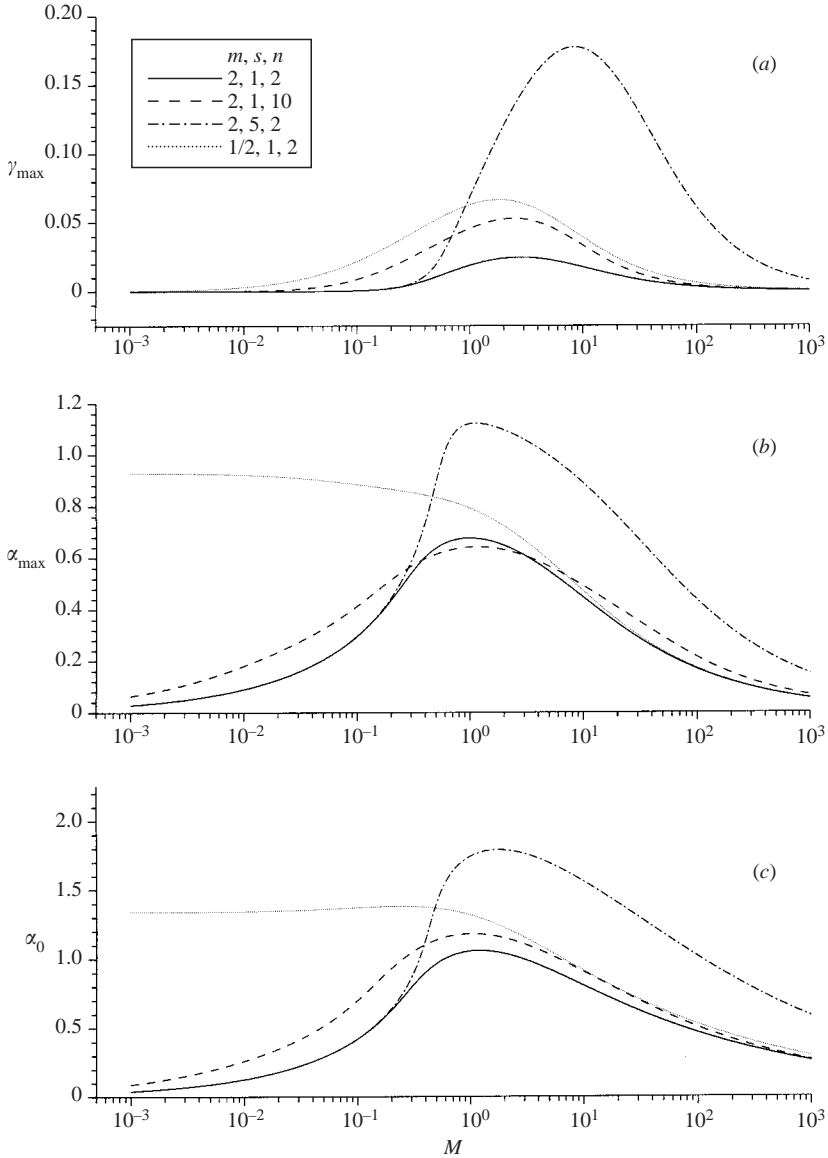FIGURE 3. (*a*) Maximum growth rate γ_{max}, (*b*) wavenumber α_{max} corresponding to the maximum growth rate, and (*c*) 'marginal-stability' wavenumber α_0 corresponding to the zero growth rate, are all bounded as functions of Marangoni number M (as shown here for a few sample parameter values given in the legend).

show $\alpha_{00}(m)$ in figure 12 below. The drop of α_{00} to zero is very steep as $m \to 1$ from below.

4.2. The growth rate increase with s

It is interesting to look for the conditions which are most favourable for achieving as strong an instability as possible. From figure 5, it transpires that γ_M grows as m decreases and as n and s increase. In fact, the solutions in the limit $m = 0$ and $n = \infty$ show that at large s, the quantities γ_M and M_M have linear asymptotics in s:
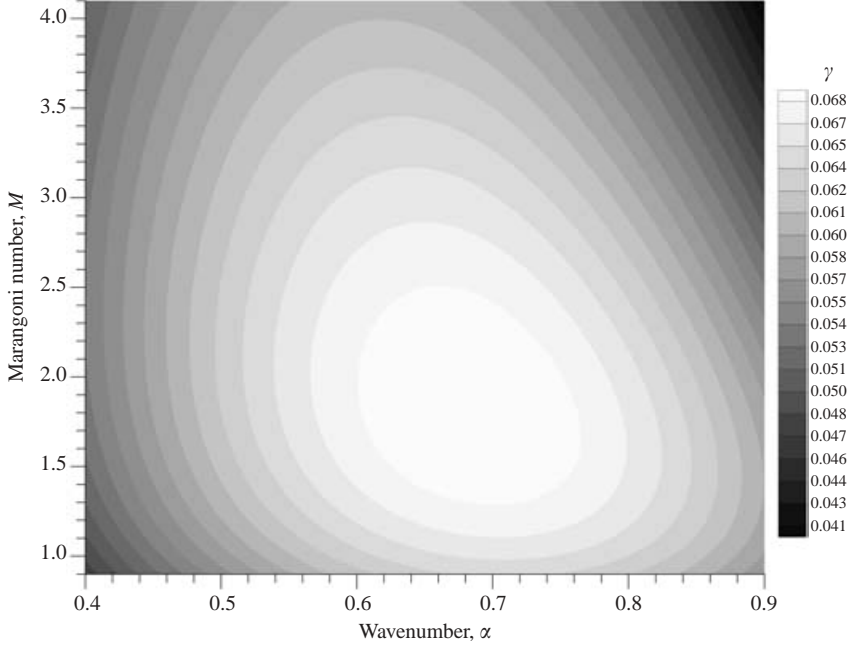
FIGURE 4. Level curves of the growth rate as a function of α and M, illustrating the fact that the growth rate always attains a maximum value γ_M for this quantity and for the values α_M and M_M corresponding to γ_M, see figures 5–7. (Here, $m = 1$, $s = 1$ and $n = 10$.)

$\gamma_M = \hat{\gamma}_M s$ and $M_M = \hat{M}_M s$ while α_M approaches a constant limit $\hat{\alpha}_M$. The asymptotic constants $\hat{\gamma}_M$, $\hat{M}_M$ and $\hat{\alpha}_M$ are found in a 'semi analytical' way, as follows.

In the limit $n \to \infty$ and for $m = 0$, the coefficients (3.20)–(3.22) of the quadratic equation (3.19) reduce to

$$q_2 = -B, \quad q_1 = s - \mathrm{i}\left(1 - \tfrac{1}{2}A - \tfrac{1}{2}AM\right), \quad q_0 = \frac{M}{4}\left(-2\alpha - \frac{1}{\alpha} + B\right) - \tfrac{1}{2}\mathrm{i}Ms, \quad (4.4)$$

where $A = 1 + s_\alpha c_\alpha/\alpha$ and $B = \alpha + c_\alpha^2/\alpha$. The equation for c_I then becomes

$$4B^3 c_I^4 - 8B^2\left(1 - \tfrac{1}{2}A - \tfrac{1}{2}AM\right)c_I^3$$
$$+ \left[Bs^2 + 5B\left(1 - \tfrac{1}{2}A - \tfrac{1}{2}AM\right)^2 + \left(-2\alpha - \frac{1}{\alpha} + B\right)B^2 M\right]c_I^2$$
$$- \left(1 - \tfrac{1}{2}A - \tfrac{1}{2}AM\right)\left[\left(1 - \tfrac{1}{2}A - \tfrac{1}{2}AM\right)^2 + \left(-2\alpha - \frac{1}{\alpha} + B\right)BM + s^2\right]c_I$$
$$- \tfrac{1}{4}Bs^2 M^2 + \tfrac{1}{2}\left(1 - \tfrac{1}{2} - \tfrac{1}{2}AM\right)\left[s^2 M + \frac{M}{2}\left(-2\alpha - \frac{1}{\alpha} + B\right)\right] = 0. \quad (4.5)$$

We substitute into this equation $M_M = \hat{M}_M s$ and $c_I = \hat{c}_I s$ and retain only the largest, s^4, terms, so that s^4 cancels out. This yields the equation

$$\hat{F}(\hat{c}_I, \hat{\alpha}, \hat{M}) = 4B^3 \hat{c}_I^4 - 8B^2 A\hat{M}\hat{c}_I^3 + \left(B - \tfrac{5}{2}BA^2\hat{M}^2\right)\hat{c}_I^2$$
$$+ \tfrac{1}{2}A\hat{M}\left(\tfrac{1}{4}A^2\hat{M}^2 + 1\right)\hat{c}_I - \tfrac{1}{4}(B + A)\hat{M}^2 = 0, \quad (4.6)$$
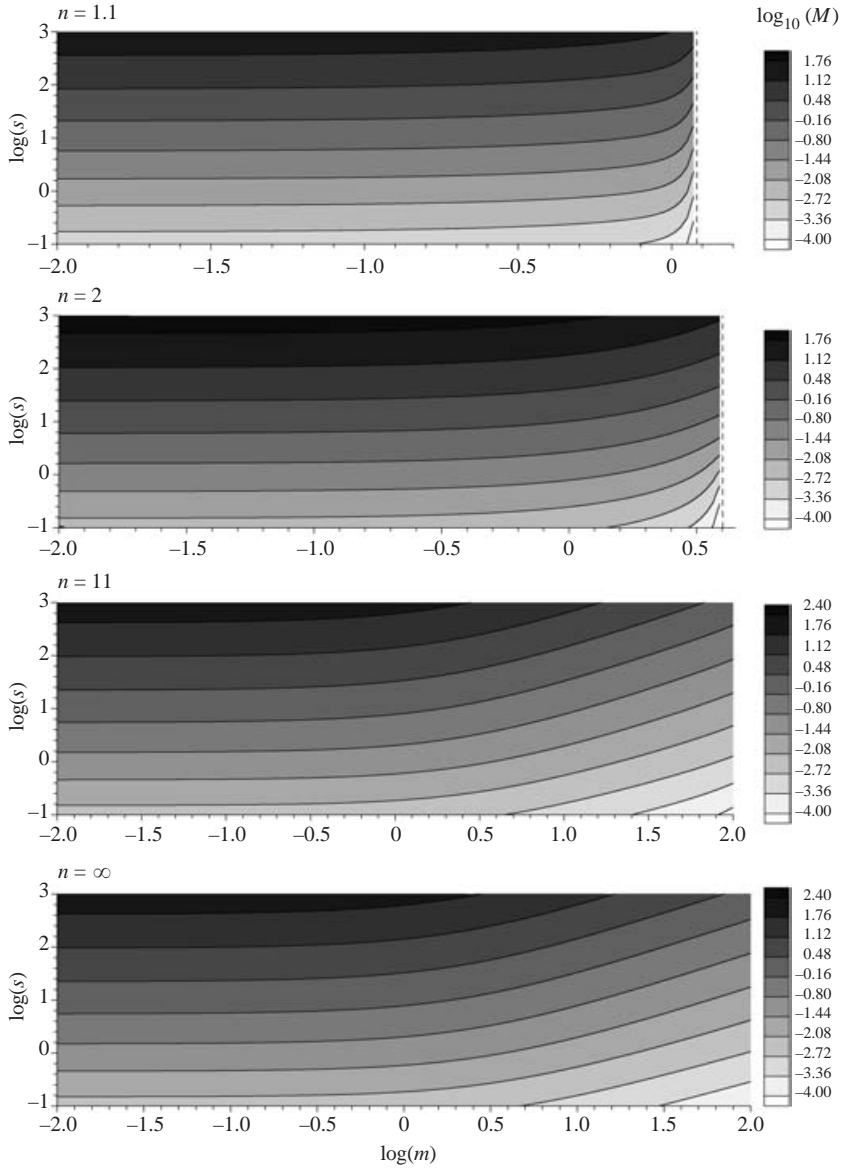
FIGURE 5. Level curves of the maximum (over all α and M) growth rate γ_M as a function of m and s for the indicated values of n. The vertical dashed line corresponds to the long-wave instability threshold $m = n^2$.

which is solved simultaneously with the 'growth-rate maximum' equations (see Appendix A)

$$\hat{\alpha}\frac{\partial \hat{F}}{\partial \hat{\alpha}} - \hat{c}_I\frac{\partial \hat{F}}{\partial \hat{c}_I} = 0 \quad \text{and} \quad \frac{\partial \hat{F}}{\partial \hat{M}} = 0.$$

The numerical solutions $\hat{\gamma}_M = 0.139$, $\hat{\alpha}_M = 1.12$, and $\hat{M}_M = 1.15$ agree with the asymptotic behaviour of the solutions of the full quadratic equation (3.19), as figure 9 shows.
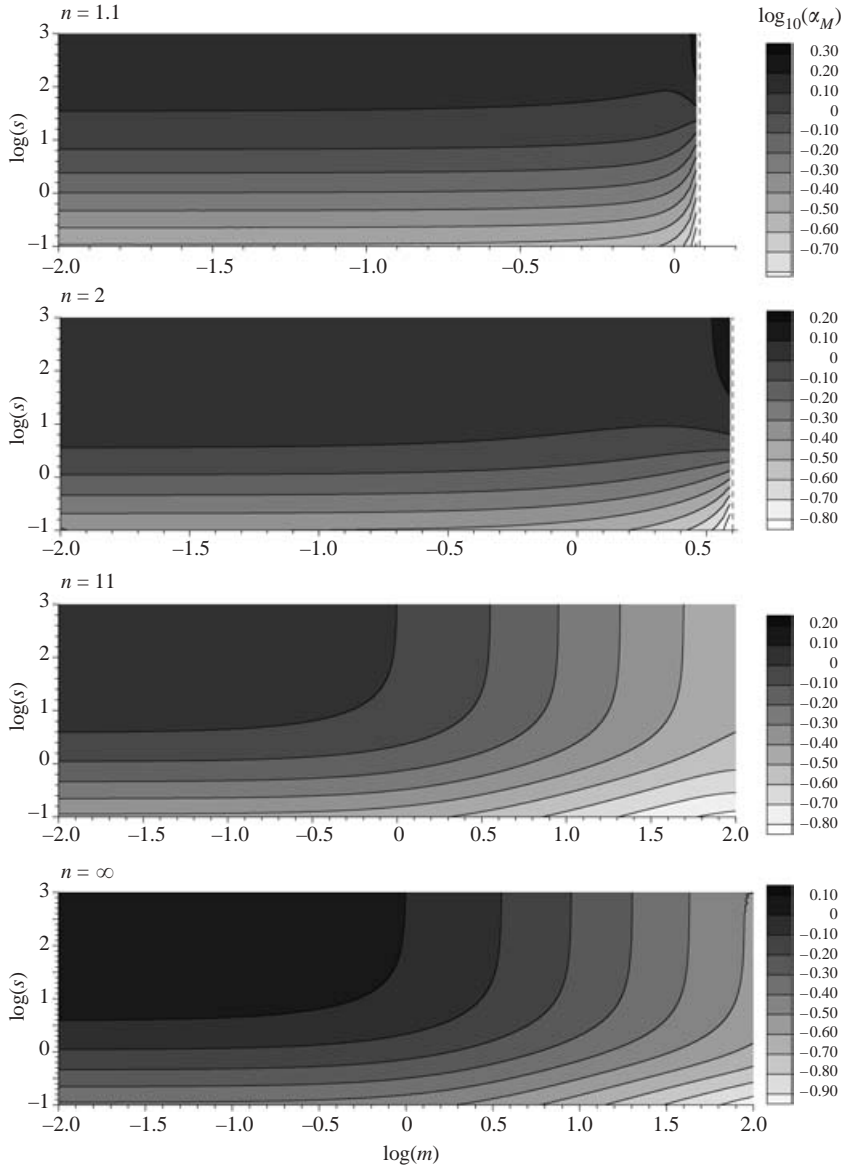
FIGURE 6. Contour plots of α_M corresponding to γ_M of figure 5.

4.3. *Long-wave and short-wave limits*

Our long-wave analytic results (Frenkel & Halpern 2002) – obtained by using the long-wave version of equation (3.11), $D^4\phi_j = 0$, and its polynomial solutions ϕ_j (which, we note, cannot be obtained from the eigenfunctions (3.12) by the simple small-α expansion of the hyperbolic functions there) – are borne out by the results of the numerical investigation of the complete quadratic equation (3.19) at small α. That paper raised a question which only the present theory can resolve. Namely, for $m \neq 1$ (no matter how close to the value $m = 1$) we found that $\gamma(\alpha) = k\alpha^2$ asymptotically near $\alpha = 0$ (with $k \to \infty$ as $m \to 1$), whereas for $m = 1$, the asymptotic behaviour is $\gamma(\alpha) = k_1\alpha^{3/2}$. This looked like a singularity of the limit $m \to 1$: the exponent jumps

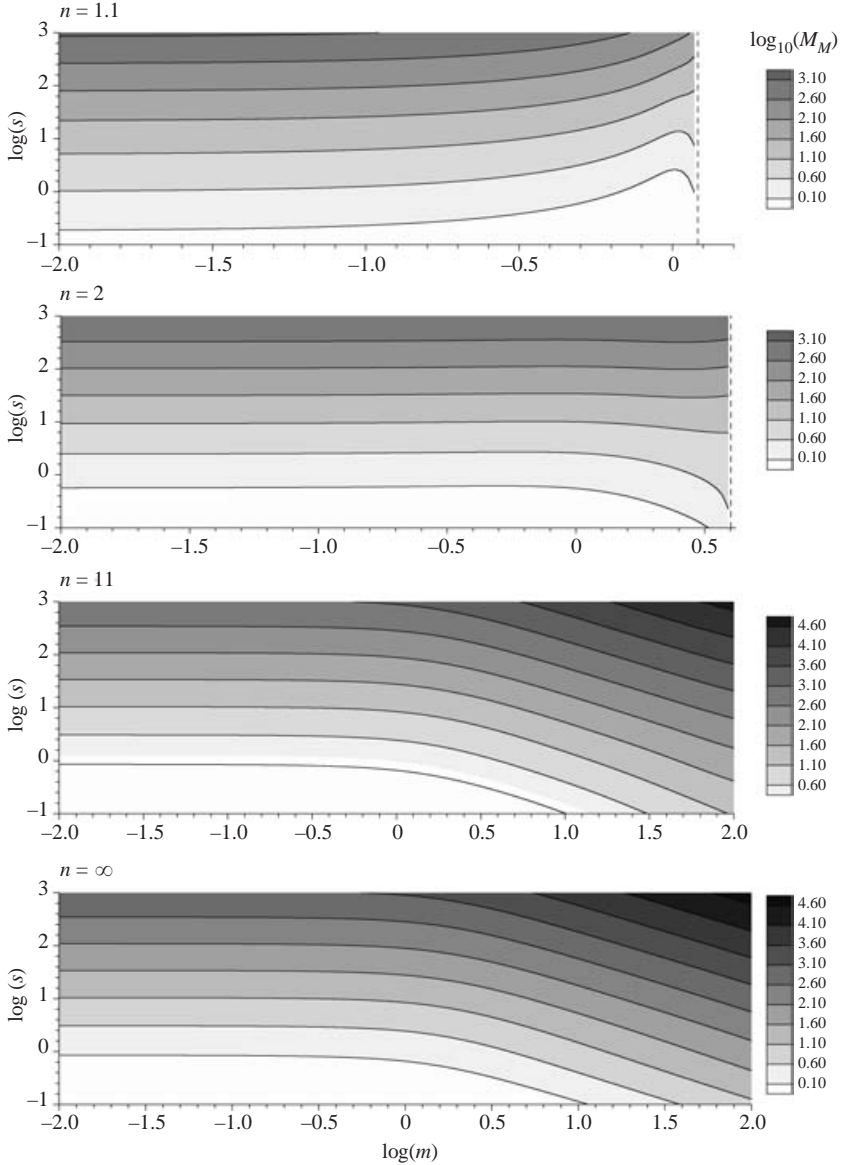FIGURE 7. Contour plots of M_M corresponding to γ_M of figure 5.

from 2 to 3/2. However, figures 5–7 do not show any discontinuity at $m = 1$, and in general it is clear that since the growth rate is obtained by solving a quadratic equation with continuous coefficients, it must be continuous at all wavenumbers and parameter values. Figure 10 suggests an explanation: the long-wave asymptotics are non-uniform with respect to small α as $m \to 1$, in the sense that the interval of α near $\alpha = 0$ for which the asymptotics yield a good approximation (say, with the relative error not exceeding 0.1) becomes smaller and smaller (see the horizontal parts of curves) as m approaches 1. At the same time, there is the interval of 'intermediate asymptotics' with $m = 1$ behaviour, $\gamma \propto \alpha^{3/2}$ – the parts of the curves which approach the slanted straight line. This interval is bounded away from zero, but expands toward
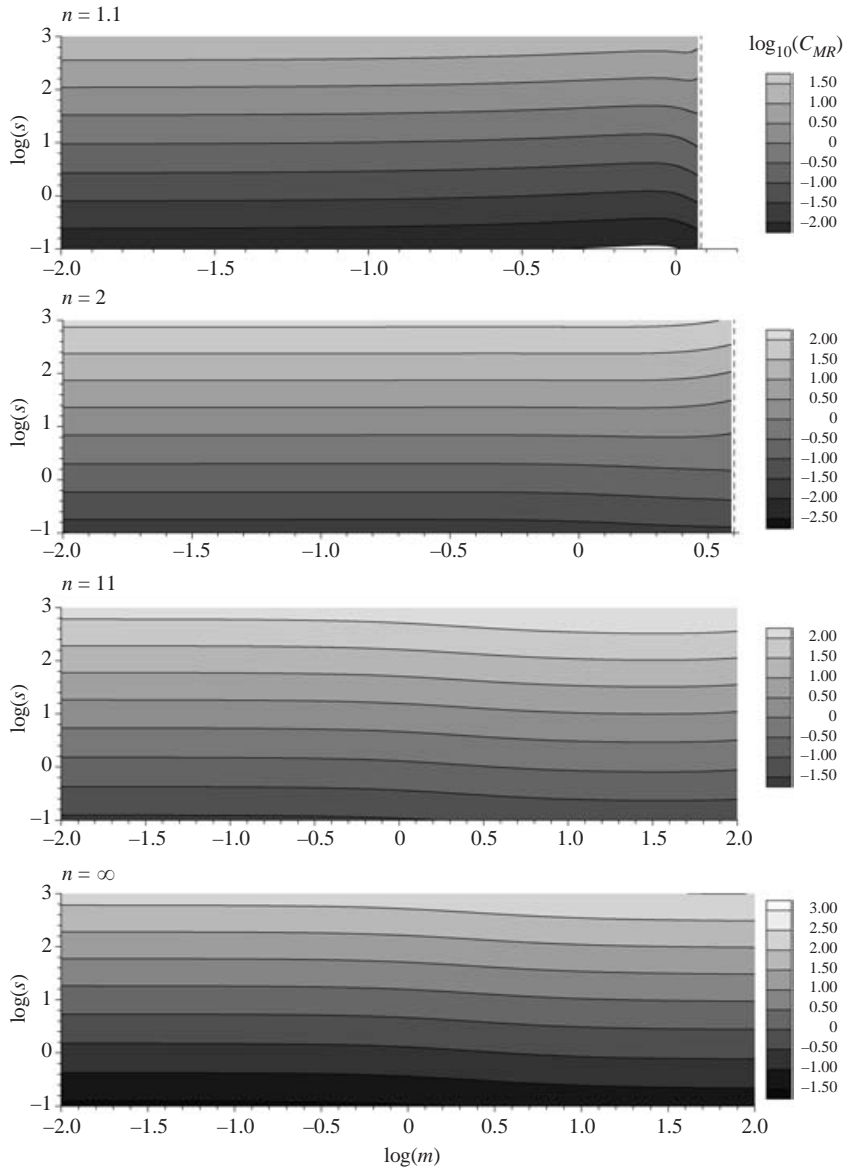
FIGURE 8. Contour plots of the wave speed c_{MR} corresponding to γ_M of figure 5.

$\alpha = 0$ as $m \to 1$, and eventually, at $m = 1$, becomes the ultimate small-α asymptotics, since then this region of the $\alpha^{3/2}$ behaviour has extended all the way to the point $\alpha = 0$. From the total continuity of the growth rate it is clear that the unstable mode changes continuously as the viscosity ratio passes through the point $m = 1$, and the same is true for the stable mode (thus, the expressions in the first two lines of table 1 of Frenkel & Halpern (2002) – although marked Mode 1 and Mode 2 there – relate to the *same* (as identified by the continuity with respect to m) mode but on the different sides of the point $m = 1$).
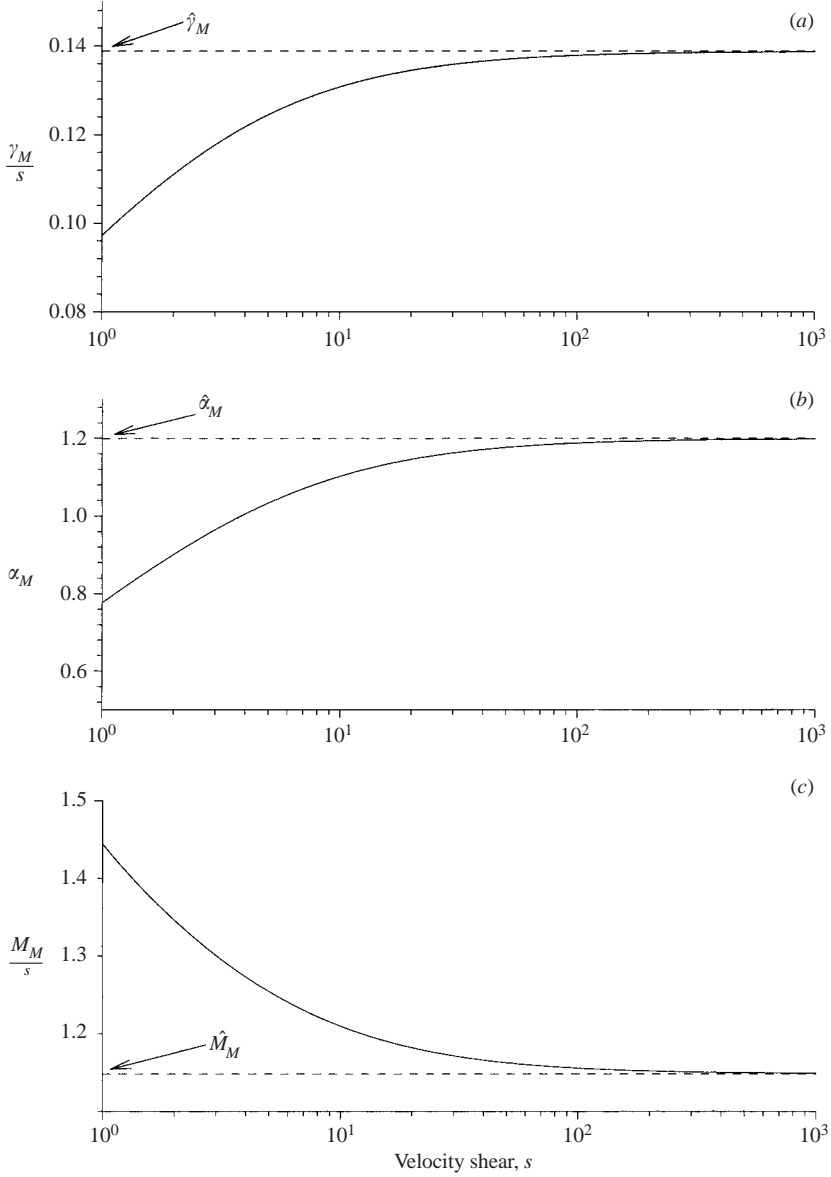
FIGURE 9. Large-s asymptotics for $n = \infty$ and $m = 0$: (a) γ_M/s, (b) α_M and (c) M_M/s versus s. The indicated asymptotic coefficients are $\hat{\gamma}_M \approx 0.139$, $\hat{\alpha}_M \approx 1.2$, and $\hat{M}_M \approx 1.14$.

We have checked that the different exponents of the long-wave power asymptotics as $n \to \infty$ and at $n = \infty$ found in Frenkel & Halpern (2002),

$$\gamma = \frac{M(n-1)}{4(1-m)}\alpha^2 \qquad\qquad\qquad \text{for } 1 < n < \infty \text{ and } m < 1, \qquad (4.7)$$

$$\gamma = \frac{(n^2 - m)(m + 3mn + 3n^2 + n^3)M}{4(m-1)(m^2 + 4mn + 6mn^2 + 4mn^3 + n^4)}\alpha^2 \quad \text{for } 1 < n < \infty \text{ and } 1 < m, \qquad (4.8)$$

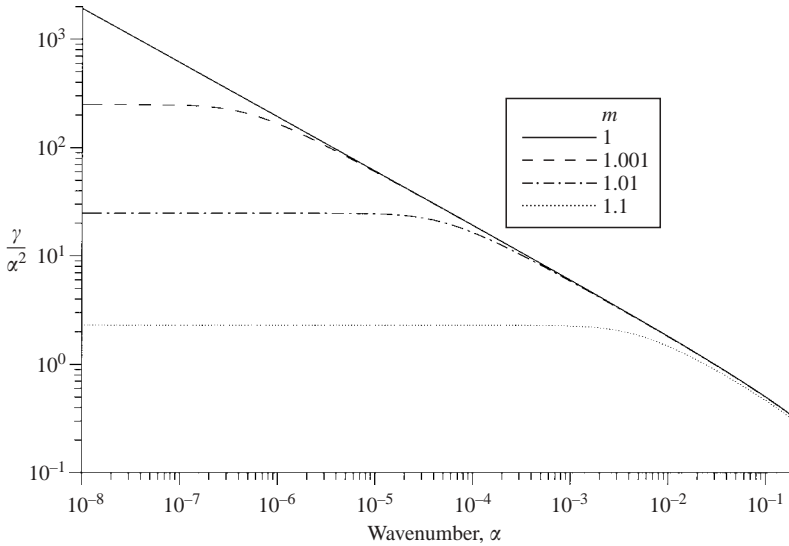$$\gamma = 1/2(M|s|)^{1/2}\alpha^{3/2} \qquad\qquad\qquad \text{for } n = \infty, \qquad (4.9)$$

FIGURE 10. Curves of γ/α^2 versus α for $M = 1$, $s = 1$, $n = 2$, and different values of m close to 1. As $m \to 1$ the $\gamma \propto \alpha^{3/2}$ asymptotic behaviour corresponding to $m = 1$ pushes back to zero the region of the $\gamma \propto \alpha^2$ behaviour characteristic of the $m \neq 1$ cases.

are explained in the same way. (We do not show here the graphs, which are similar to figure 10.) It is clear that a similar non-uniformity of small-α asymptotics should exist with respect to the Marangoni number M in the limit $M \to \infty$. Indeed, some asymptotic coefficients are proportional to a positive power of M, and therefore the growth rate would have reached arbitrarily large values as $M \to \infty$ for any (hypothetical) fixed $\alpha = \alpha_v$ if the asymptotic formula had held at α_v for all M. However, we know that the growth rate as a function of M (with all its other arguments being fixed) is bounded.

A somewhat similar phenomenon is illustrated in figure 11 for $s \to 0$. The long-wave theory (Frenkel & Halpern 2002) indicates, for the values of parameters used there, the asymptotic small-α behaviour $\gamma = k_2\alpha^2$ for $s \neq 0$ and $\gamma = -k_3\alpha^3$ for $s = 0$, with positive constants k_2 and k_3. At $s = 0$, the α-interval of α^2 asymptotics has degenerated into the single point $\alpha = 0$, and the interval of α^3 (stable) asymptotics starts immediately at $\alpha = 0$, in contrast to being bounded away from $\alpha = 0$ when $s \neq 0$.

The transition from instability to stability has a somewhat different character as $M \to 0$ for $m < 1$. As is clear from figure 12, the marginal wavenumber stays finite as $M \to 0$, which is in contrast to the transition to stability via $s \to 0$ (see figure 11). However, at $M = 0$, the less stable of the two modes has growth rate equal to zero for all wavenumbers. (This is clear from equation (A 3) because $q_{0R} = q_{0I} = 0$ for this case.) Thanks to this, the transition to stability is not of a singular-limit type in this case as well.

We have checked that the transition to stability on the other boundaries of the instability region in the parameter space, namely (i) $M \to 0$ for $m > 1$, (ii) $n \to 1$ and (iii) $m \to n^2$ for $M < 5/2$ are of the same type as the one for $s \to 0$ (see figure 11). In fact, the relevant long-wave asymptotics, which can be obtained from equation (A 3), are, in addition to equations (4.7) and (4.8), the following equations (which were not
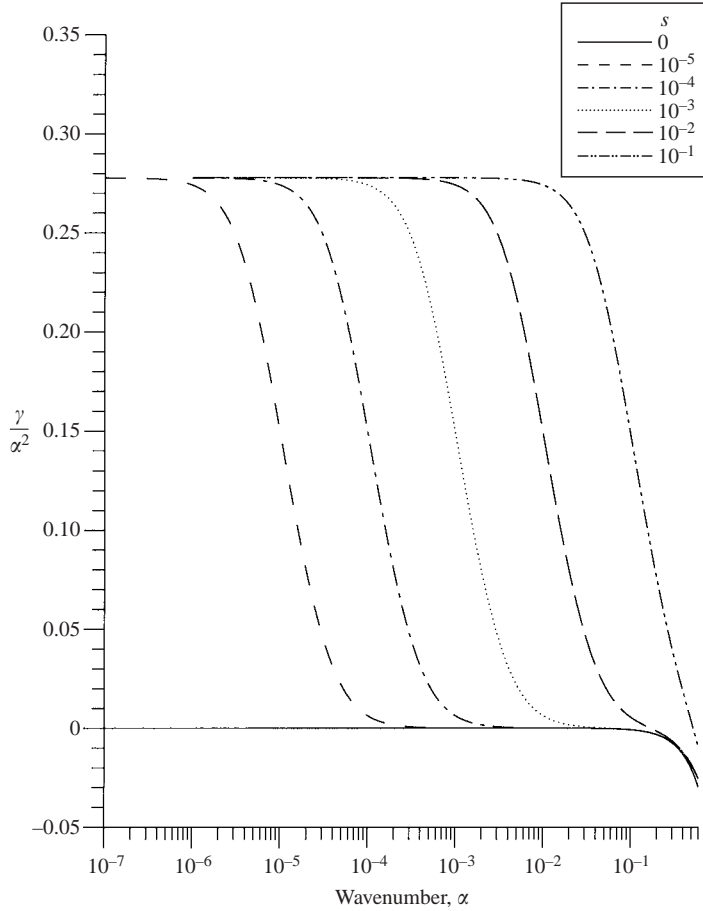
FIGURE 11. As $s \to 0$, the $\gamma \propto \alpha^3$ asymptotic growth rate behaviour corresponding to $s = 0$ (solid line) 'compresses' back to zero the region of the $\gamma \propto \alpha^2$ behaviour characteristic of $s \neq 0$ cases (with $n = 2$, $m = 0.1$ and $M = 1$).

obtained in Frenkel & Halpern 2002):

$$\gamma = -\frac{M(1+m)\alpha^2}{1+14m+m^2} \qquad \text{for } n = 1 \text{ and } m < 1, \tag{4.10}$$

$$\gamma = -\frac{M^2 s^2(m+1)\alpha^6}{192(m-1)^2} \qquad \text{for } n = 1 \text{ and } m > 1, \tag{4.11}$$

$$\gamma = -\frac{M\alpha^2}{4(1+n)} \qquad \text{for } m = n^2 \text{ and } M < \tfrac{5}{2}, \tag{4.12}$$

$$\gamma = \frac{(2M-5)n\alpha^4}{60(1+n)} \qquad \text{for } m = n^2 \text{ and } M > \tfrac{5}{2}. \tag{4.13}$$

Equation (4.13) indicates long-wave instability for $m = n^2$. This instability then should persist for some interval of larger m, such that $m > n^2$. However, the long-wave asymptotic expression (4.8) asserts (long-wave) stability for $m > n^2$. Nevertheless the instability does exist, but the α-interval of instability is *bounded away from zero*
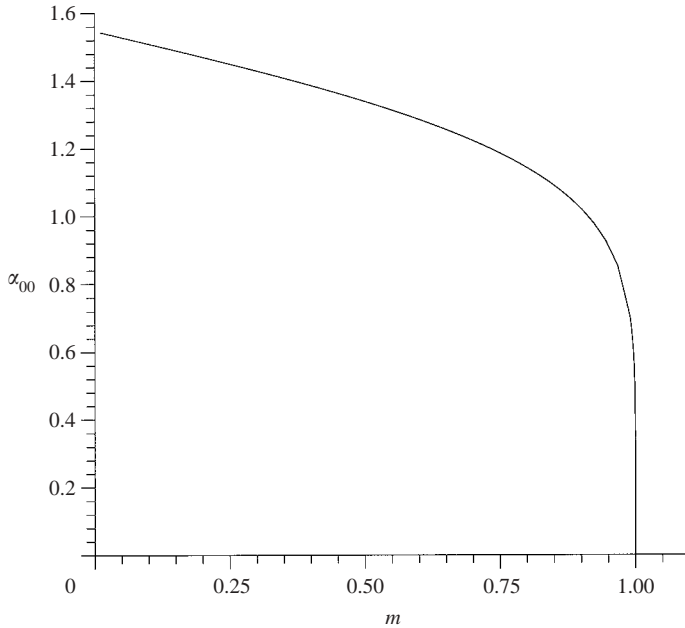
FIGURE 12. The $M \to 0$ limit value of marginal wavenumber α_{00} versus the viscosity ratio m. (Here, $n = 10$ and $s = 1$.)

(see inset in figure 2*a*). The critical value of m is then not n^2 but some greater number $m_c(s, n, M) > n^2$. We can find the function $m_c(s, n, M)$ by noticing that at criticality both the growth rate and its derivative with respect to α are zero (because the growth rate is zero at its maximum). With the zero growth rate, $c_I = 0$, equation (A 3) becomes $F = q_2 q_{0I}^2 - q_{1R} q_{0I} q_{1I} + q_{0R} = 0$ and the first equation of (A 4) becomes $\partial F / \partial \alpha = 0$. These are two equations for five unknowns: m, n, M, s and α. We solve them to find the critical values $m_c(s, n, M)$ and $\alpha_c(s, n, M)$. They are shown respectively in figures 13 and 14. (Actually, in figure 13 we show the level curves of the 'deviation quantity' $(m_c - n^2)/n^2$ which is zero if $m_c = n^2$.) One can see that both these quantities grow as s increases to infinity and n decreases to $n = 1$. At smaller s and $(n - 1)$, the deviation becomes so small that we fail to compute these small values, especially at larger M. This is why there are empty spaces near the left-hand boundaries of some parts of figures 13 and 14. It is clear from figure 13 that in the region of mid-wave instability there is a minimum threshold value of s for the instability, in contrast to the all-s instability for the region $m < n^2$.

In the short-wave limit, $\alpha \to \infty$, equation (A 3) becomes, to the leading order,

$$4c_I^4(m+1)^4 + 4c_I^3(m+1)^3(M+1) + c_I^2(m+1)^2 \left(M + \tfrac{5}{4}(m+1)^2\right)$$

$$+ \tfrac{1}{8}c_I(m+1)(M+1)\left[M^2 + 6M + 1\right] + \tfrac{1}{16}M(M+1)^2 = 0. \quad (4.14)$$

The largest solution is $c_I = -M/(2(m+1))$, independent of s and n. Thus, the system is stable at large α, with the growth rate of the least-stable mode being asymptotically linear:

$$\gamma_{\alpha \to \infty}(\alpha) \sim -\frac{\min(M, 1)}{2(m+1)} \alpha. \quad (4.15)$$

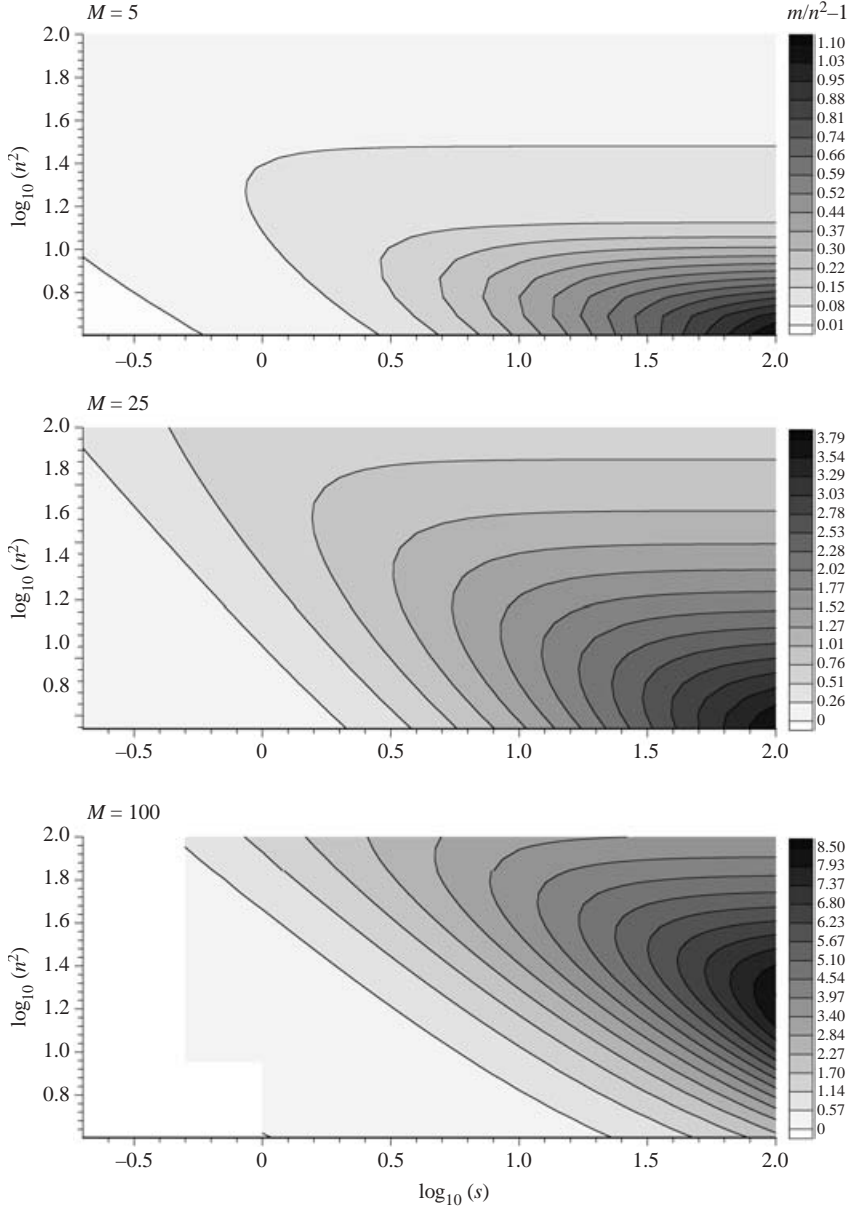This is corroborated by numerical solution of the exact equation (3.19).

FIGURE 13. Critical manifold deviates from $m = n^2$ for $M > 5/2$: level curves of the relative deviation $(m_c - n^2)/n^2$ as a function of s and n^2 for the indicated values of M.

In conclusion, as was mentioned before, there is continuity of growth rate for all wavenumbers and all parameter values, including the limiting cases $m = 1$ and $n = \infty$, as well as the boundaries of the instability region in the space of parameters. For mathematical completeness, the less realistic limit $\sigma_0 \to 0$ is considered in Appendix D, where we show that the convergence of the dispersion function is non-uniform at large wavenumbers.
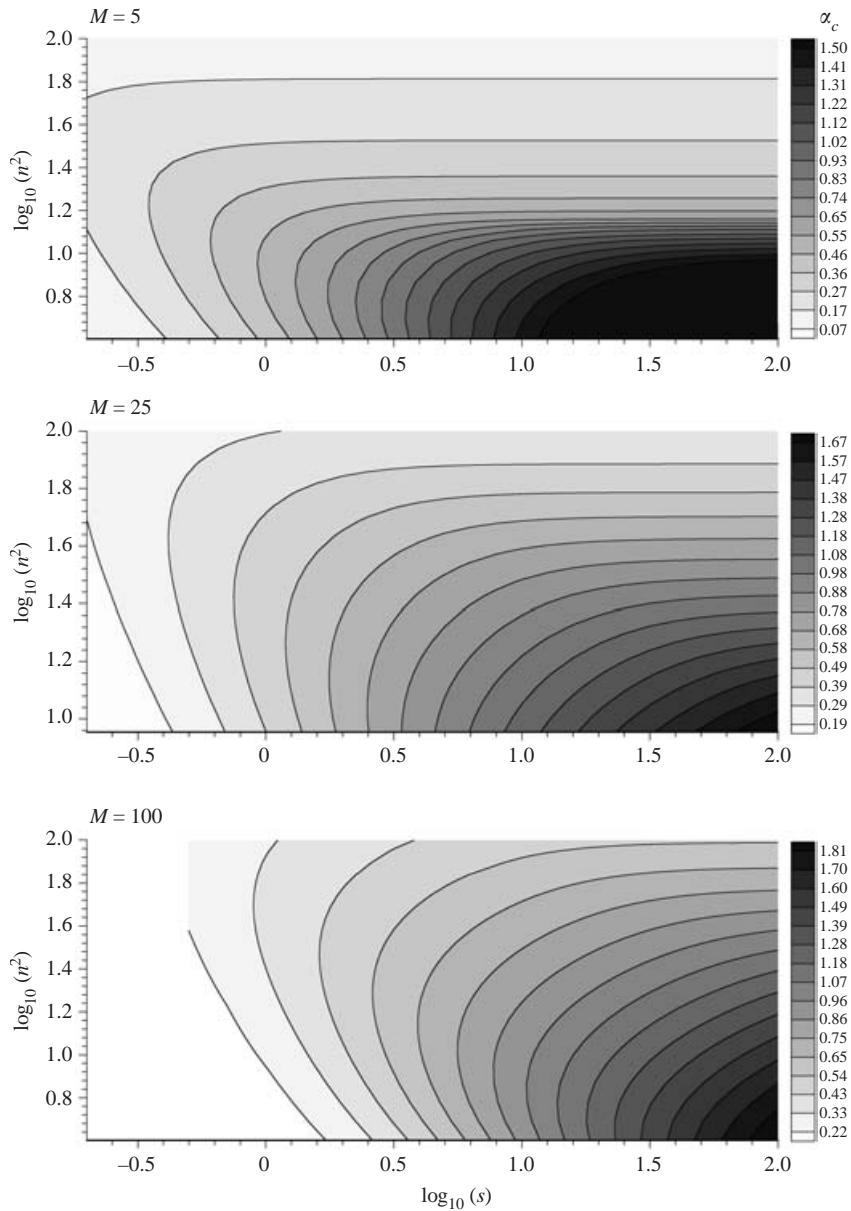
FIGURE 14. Level curves of the critical wavenumber α_c as a function of s and n^2 for the indicated values of M.

5. Conclusions and discussion

The non-inertial instability due to the presence of both the interfacial surfactant and velocity shear in a two-layer planar flow of the Couette–Poiseuille type, readily admits a numerical (not requiring more than solving a quadratic equation) and asymptotic investigation over the entire range of wavenumbers and in the entire space of the Marangoni number M, the velocity shear s, the viscosity ratio $m(>0)$, and the thickness ratio $n(\geqslant 1)$. Unlike the well-known instabilities of similar plane Couette–Poiseuille flows without surfactants which are due to inertia effects, it does

not require the interfacial jump of viscosity or of any other bulk fluid property; in particular, it persists for $m = 1$. In all cases, this instability disappears if $s = 0$ or $M = 0$.

If $M < 5/2$, the system is unstable if $m < n^2$ and $n > 1$, and stable otherwise. (It is interesting to note that the criticality $m = n^2$ appeared, for a different instability, in Yiantsios & Higgins 1988.) The instability takes place for the interval of wavenumbers $0 < \alpha < \alpha_0$, where α_0 is not greater than 1 in order of magnitude for realistic parametric regimes. The growth rate has a single maximum γ_{max} at $\alpha = \alpha_{max}$ (the latter being less than or – frequently – equal to 1 in order of magnitude), and α_0/α_{max} is of magnitude-order 1 except for certain unrealistic parameter ranges where it is large (see the case of extremely small surface tension in Appendix D).

Moreover, the positive growth rate has a single maximum γ_M at a point (α_M, M_M) on the (α, M)-plane. This grows without any bound as m decreases to 0, s grows to ∞, and n grows to ∞. In the limit $m = 0$ and $n = \infty$, the asymptotic growths of γ_M and M_M with s are linear while α_M is asymptotically constant as $s \to \infty$.

For $M > 5/2$, the instability occurs even for some $m > n^2$, and then in a mid-wave range of wavenumbers $0 < \alpha_1 < \alpha < \alpha_0$, bounded away from zero. In this mid-wave case only, there is a minimum threshold value of s for the instability.

The growth rate of the unstable mode (one of the two fundamental normal modes for every wavenumber in the present linear theory) is continuous everywhere (including such limits as $m \to 1$, $s \to 0$, $n \to \infty$ or $M \to \infty$ for which the long-wave theory seems – misleadingly – to suggest singularities). However, the convergence of the dispersion function to its limit is non-uniform at small α for certain parametric limits, and for the limit of vanishing surface tension it is non-uniform at large α.

The numerical solutions confirm that the small-α growth rate behaves like α^2 for $m \neq 1$ and $\alpha^{3/2}$ for $m = 1$ if $s \neq 0$. For $s = 0$, the less-stable mode decays at a rate asymptotically $\propto \alpha^4$ at small α. In the short-wave limit, $\alpha \to \infty$, the decay rate changes only linearly with α.

Finally, we note that in the limit $M \to \infty$ in which the surface becomes immobilized by the surfactant monolayer, the growth rate approaches zero.

As is usual when simplified equations are used, one should check that the consistency conditions have been satisfied. In our case, the Stokes approximation, the consistency conditions clearly demand that the neglected inertia terms, the right-hand sides of equations (3.5) with the Stokes approximation results substituted for $c(\alpha)$ and $\phi_j(\alpha)$, must be much smaller than the terms on the corresponding left-hand sides of equations (3.5). This can be verified for each specific set of parameters, but it seems difficult to obtain any general parametric conditions that apply for all possible Couette–Poiseuille flows at once. However, it is clear that the right-hand side of equation (3.5) can be made as small as desired by decreasing the non-Stokes parameter Re/Ca there.

The physical mechanism of the instability has already been discussed in Frenkel & Halpern (2002); we include it here for completeness. It is illuminated by considering the ratio g/h (of the surfactant concentration amplitude to displacement amplitude) for the case of plane Couette flow with $m = 1$ and large n. In figure 15 the unstable and stable modes with $\alpha = 0.5$ for $M = 1$, $s = 1$, $n = 10$ are presented. For small α, one can see that $g/h \approx s/c \propto \pm e^{i\pi/4}$, where the negative sign corresponds to the growing mode. Hence, for the growing mode, the surfactant concentration and the interface disturbance are out of phase by approximately $5\pi/4$, which is quite close to π (see figure 15a), while for the decaying mode, the phase shift is $\pi/4$, which is closer to 0 (see figure 15b). So, for the growing mode, the surfactant concentration is a minimum, and thus the surface tension a maximum, approximately where the lower
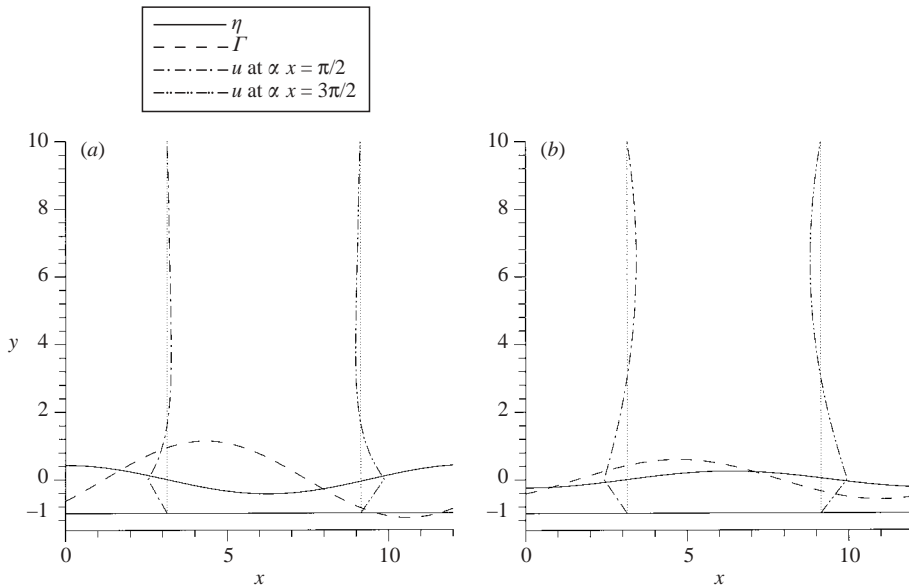
FIGURE 15. (a) Unstable and (b) stable modes for $M = 1$, $m = 1$, $s = 1$, $n = 10$ and $\alpha = 0.5$. Solid curve: the perturbed interface; dashed curve: the disturbance of the surfactant concentration; dash-dotted curves: the profile of the (scaled) horizontal component of velocity disturbance at the locations $\alpha x = \pi/2$ and $\alpha x = 3\pi/2$. (The dotted vertical lines are to guide the eye).

layer, the film, is thickest; and it is a maximum (surface tension minimum) where the film is thinnest. Thus there is a surface tension increase, and hence a flow, from troughs to peaks, which clearly causes the thickness difference to grow. In contrast, for the stable mode, the spatial variations of the surfactant concentration and the interface are almost in phase, so there is now a fluid flow in the film from its peaks to troughs. This causes the disturbances to decay.

It is interesting to note that for the particular case of purely Couette flow, where the velocity profiles are linear, there are well-known exact analytical solutions (in terms of integrals with Airy functions: see von Mises 1912 and Hopf 1914, as cited in Drazin & Reid 1981; see also Hooper 1985 and Joseph & Renardy 1993) of the unreduced Orr–Sommerfeld equations (3.5) which include the full inertia terms. This would allow one to consider the influence of inertia on the instability. However, earlier experience with such exact solutions suggests that the deduction of tractable results from them is likely to be feasible only for certain asymptotic limits (Drazin & Reid 1981).

Since the present theory has shown the instability of the general Couette–Poiseuille flow to require only a non-zero velocity shear at the interface, it is tempting to conjecture that such an instability will be present in other flows with an insoluble surfactant monolayer, even when such flows have (perhaps, slightly) curved interfaces, such as those in the (cylindrical) Couette flow of two fluids in a thin gap between coaxial rotating cylinders. We hope to investigate this question in more detail elsewhere.
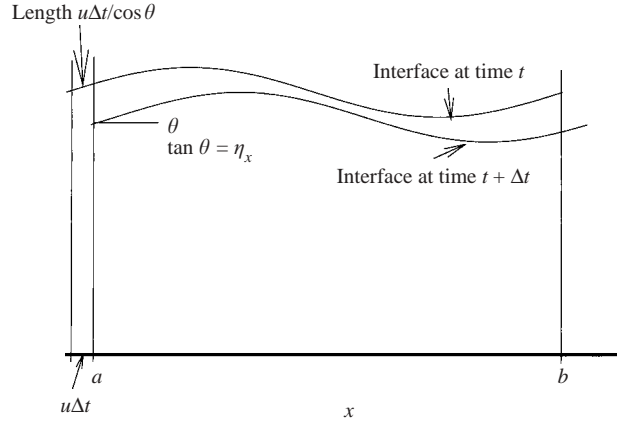
FIGURE 16. Displacement of the interface from time t to $t + \Delta t$.

Appendix A. Equations for the growth rate

The growth rate is $\gamma = \alpha c_I$ where c satisfies the equation

$$q_2 c^2 + q_1 c + q_0 = 0. \tag{A 1}$$

By taking the imaginary part of this equation, c_R can be expressed in terms of c_I:

$$c_R = \frac{q_{1R} c_I + q_{0I}}{2 q_2 c_I + q_{1I}}, \tag{A 2}$$

where $q_0 = q_{0R} + i q_{0I}$ and $q_1 = q_{1R} + i q_{1I}$. The above expression for the wave speed is then substituted into the equation obtained by taking the real part of (A 1), which yields the following equation for c_I:

$$F(c_I, \alpha, M; s, m, n) = -4 q_2^3 c_I^4 - 8 q_2^2 q_{1I} c_I^3 + \left(4 q_{0R} q_2 - 5 q_{1I}^2 - q_{1R}^2\right) q_2 c_I^2$$
$$+ \left(4 q_{0R} q_2 - q_{1R}^2 - q_{1I}^2\right) q_{1I} c_I + q_2 q_{0I}^2 - q_{1R} q_{0I} q_{1I} + q_{0R} q_{1I}^2 = 0. \tag{A 3}$$

The growth rate attains a maximum at some α and M. At this maximum, $\partial \gamma / \partial \alpha = \partial \gamma / \partial M = 0$ (where $\gamma = \alpha c_I$), which become

$$\alpha \frac{\partial F}{\partial \alpha} - c_I \frac{\partial F}{\partial c_I} = 0, \quad \frac{\partial F}{\partial M} = 0, \tag{A 4}$$

by using $c_I(\alpha, M)$ as is implicitly defined by (A 3). Equations (A 3) and (A 4) enable us to determine the quantities c_I, α and M corresponding to the maximum rate of growth, given the values of m, s and n (see figures 5–8).

Appendix B. Derivation of the surfactant equation for the case $\Gamma = \Gamma(x, t)$

First, for simplicity, disregard diffusion, $D_s = 0$, and consider the change ΔN from time t to $t + \Delta t$ in the amount of surfactant $N = \int_a^b \Gamma \sqrt{1 + \eta_x^2} \, dx$ contained on the strip of the interface (of unit width) between the fixed boundaries $x = a$ and $x = b$ (figure 16). For small Δt we have

$$\Delta N = \Delta t \int_a^b \frac{\partial}{\partial t} \left(\Gamma \sqrt{1 + \eta_x^2}\right) dx + O(\Delta t^2). \tag{B 1}$$

On the other hand, $\Delta N = F(a, t)\Delta t - F(b, t)\Delta t$ where $F(x_0, t)$ is the rate at which the surfactant crosses from the left of $x = x_0$ to the right of it. This depends on the x-component u of the interfacial velocity at x_0 (see figure 16). During the time interval Δt, it moves through the boundary $x = a$, the small piece of interface corresponding to the x interval between $x = a$ and $x = a - u\Delta t$. This piece, because of the interfacial slope $\tan\theta = \eta'(a, t)$, has the length (up to errors of $O(\Delta t^2)$) $\Delta x / \cos\theta = u\Delta t \sqrt{1 + \eta_x^2}$, and thus contains the following amount of the surfactant:

$$F(a, t)\Delta t = \Gamma(a, t)u(a, \eta(a), t)\Delta t \sqrt{1 + \eta_x^2(a, t)}. \tag{B 2}$$

Similarly, $F(b, t) = \Gamma(b, t)u(b, \eta(b), t)\sqrt{1 + \eta_x^2(b, t)}$. So,

$$\Delta N = \Delta t \left(\Gamma(a, t)u(a, t)\sqrt{1 + \eta_x^2(a, t)} - \Gamma(b, t)u(b, t)\sqrt{1 + \eta_x^2(b, t)} \right) + O(\Delta t^2)$$

$$= \Delta t \left(-\int_a^b \frac{\partial}{\partial x} \left(\Gamma(x, t)u(x, t)\sqrt{1 + \eta_x^2(x, t)} \right) \mathrm{d}x \right) + O(\Delta t^2), \tag{B 3}$$

where $u(x, t) := u(x, \eta(x, t), t)$, a function of x and t only. Equating the two expressions for ΔN, (B 1) and (B 3), and considering the limit $\Delta t \to 0$, we obtain

$$\int_a^b -\frac{\partial}{\partial x} \left(\Gamma(x, t)u(x, t)\sqrt{1 + \eta_x^2(x, t)} \right) \mathrm{d}x = \int_a^b \frac{\partial}{\partial t} \left(\Gamma(x, t)\sqrt{1 + \eta_x^2(x, t)} \right) \mathrm{d}x.$$

This equality, since it holds for all a and b, implies

$$\frac{\partial}{\partial t} \left(\Gamma \sqrt{1 + \eta_x^2} \right) + \frac{\partial}{\partial x} \left(\Gamma u \sqrt{1 + \eta_x^2} \right) = 0, \tag{B 4}$$

where $u = u(x, \eta(x, t), t) = u(x, t)$ is the x-component of velocity at the interface, the latter being parameterized by x.

Bringing back the diffusion, one must take into consideration that there is a corresponding contribution to ΔN because, during the time interval between t and $t + \Delta t$ there is a certain amount of surfactant crossing from the left to the right through the material point of the interface which has $x = a$ at time $t + \Delta t$, that is $x = a - u\Delta t$ at time t. This amount, up to errors $O(\Delta t)^2$, is given by

$$\left(-D_s \frac{\partial \Gamma}{\partial l} \right) \Delta t \quad \left(\text{where } \frac{\partial}{\partial l} = \frac{1}{\sqrt{1 + \eta_x^2}} \frac{\partial}{\partial x} \right),$$

and must be added into equation (B 2); a similar term appears at $x = b$. This leads to the equation accounting for the presence of diffusion:

$$\frac{\partial}{\partial t} \left(\Gamma \sqrt{1 + \eta_x^2} \right) + \frac{\partial}{\partial x} \left(\Gamma u \sqrt{1 + \eta_x^2} \right) = D_s \frac{\partial}{\partial x} \left(\frac{1}{\sqrt{1 + \eta_x^2}} \frac{\partial \Gamma}{\partial x} \right). \tag{B 5}$$

Appendix C. Squire's Theorem

For three-dimensional normal modes, equation (3.1) changes to

$$(\tilde{u}_j, \tilde{v}_j, \tilde{w}_j, \tilde{p}_j, \tilde{\eta}, \tilde{\Gamma}) = [U_j(y), V_j(y), W_j(y), f_j(y), h, g]\mathrm{e}^{\mathrm{i}\alpha x + \beta z - Gt} \tag{C 1}$$

(where $\tilde{u}_j$, $\tilde{v}_j$ and $\tilde{w}_j$ are the x-, y- and z-components of velocity disturbances). The governing problem is as follows:

$$\mathrm{i}\alpha f_1 = (-\alpha^2 - \beta^2 + \mathrm{D}^2)U_1, \quad \mathrm{i}\alpha f_2 = m(-\alpha^2 - \beta^2 + \mathrm{D}^2)U_2 \tag{C 2}$$

(x-momentum Stokes' equations);

$$\mathrm{D}f_1 = (-\alpha^2 - \beta^2 + \mathrm{D}^2)V_1, \quad \mathrm{D}f_2 = m(-\alpha^2 - \beta^2 + \mathrm{D}^2)V_2 \qquad (\mathrm{C}\,3)$$

(y-momentum Stokes' equations);

$$\mathrm{i}\beta f_1 = (-\alpha^2 - \beta^2 + \mathrm{D}^2)W_1, \quad \mathrm{i}\beta f_2 = m(-\alpha^2 - \beta^2 + \mathrm{D}^2)W_2 \qquad (\mathrm{C}\,4)$$

(z-momentum Stokes' equations);

$$\mathrm{i}\alpha U_1 + \mathrm{i}\beta W_1 + \mathrm{D}V_1 = 0, \quad \mathrm{i}\alpha U_2 + \mathrm{i}\beta W_2 + \mathrm{D}V_2 = 0 \qquad (\mathrm{C}\,5)$$

(incompressibility equations);

$$U_1 = V_1 = W_1 = 0 \quad \text{at} \quad y = -1, \quad U_2 = V_2 = W_2 = 0 \quad \text{at} \quad y = n \qquad (\mathrm{C}\,6)$$

(no-slip conditions);

$$U_1(0) + sh = U_2(0) + \frac{s}{m}h, \quad V_1(0) = V_2(0), \quad W_1(0) = W_2(0) \qquad (\mathrm{C}\,7)$$

(velocity continuity equations);

$$-\mathrm{i}Gh = V_1(0) \qquad (\mathrm{C}\,8)$$

(kinematic condition);

$$\mathrm{i}Gg + \mathrm{i}\alpha\,[sh + U_1(0)] + \mathrm{i}\beta W_1(0) = 0 \qquad (\mathrm{C}\,9)$$

(surfactant equation);

$$-2\,[m\mathrm{D}V_2(0) - \mathrm{D}V_1(0)] + f_2(0) - f_1(0) = \left(-\alpha^2 - \beta^2\right)h \qquad (\mathrm{C}\,10)$$

(normal-stress balance);

$$m\,[\mathrm{D}U_2(0) + \mathrm{i}\alpha V_2(0)] - \mathrm{D}U_1(0) - \mathrm{i}\alpha V_1(0) = \mathrm{i}\alpha Mg \qquad (\mathrm{C}\,11)$$

(tangential-stress balance in the x-direction);

$$m\,[\mathrm{D}W_2(0) + \mathrm{i}\beta V_2(0)] - \mathrm{D}V_1(0) - \mathrm{i}\beta V_1(0) = \mathrm{i}\beta Mg \qquad (\mathrm{C}\,12)$$

(tangential-stress balance in the z-direction).

It is straightforward to check that for every solution

$$(\alpha, \beta, G, U_1, V_1, W_1, U_2, V_2, W_2, f_1, f_2, h, g) \qquad (\mathrm{C}\,13)$$

there is a two-dimensional solution

$$(\hat{\alpha}, \hat{\beta} = 0, \hat{G}, \hat{U}_1, \hat{V}_1, \hat{W}_1 = 0, \hat{U}_2, \hat{V}_2, \hat{W}_2 = 0, \hat{f}_1, \hat{f}_2, \hat{h}, \hat{g}) \qquad (\mathrm{C}\,14)$$

of the problem with transformed parameters $\hat{m}$, $\hat{n}$, $\hat{s}$, $\hat{M}$ such that

$$\hat{G} = G, \quad \hat{\alpha}^2 = \alpha^2 + \beta^2, \quad \hat{\alpha}\hat{U}_j = \alpha U_j + \beta W_j, \quad \hat{V}_j = V_j, \quad \hat{f}_j = f_j, \quad \hat{h} = h, \quad \hat{g} = g, \tag{C\,15}$$

and

$$\hat{m} = m, \quad \hat{n} = n, \quad \hat{\alpha}\hat{s} = \alpha s, \quad \hat{M} = M. \qquad (\mathrm{C}\,16)$$

The two-dimensional mode has the same growth rate as the three-dimensional one. Therefore, if the three-dimensional mode is unstable (i.e. the growth rate $\mathrm{Im}\,G > 0$) at some set of parameter values, then there is an (equally) unstable two-dimensional mode for a smaller value $\hat{s}$ of s (since $\hat{\alpha} \geqslant \alpha$), with the values of all the other parameters being identical.
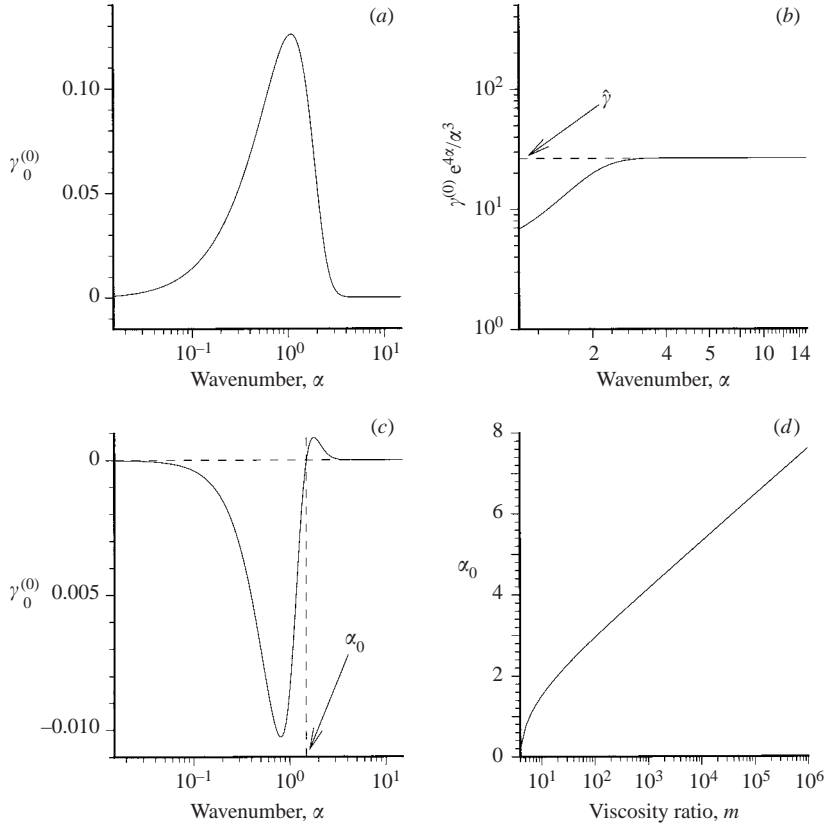
FIGURE 17. (a) For zero basic surface tension, $\sigma_0 = 0$, the growth rate $\gamma_0^{(0)}$ is positive for all wavenumbers if $m < n^2$ Here, $m = 0.1$. (b) Large-α behaviour, where the indicated asymptotic coefficient $\hat{\gamma} = 64/(M^{(0)}(m+1)^2)$. Here, $m = 0.1$. (c) For $m > n^2$, the growth rate has a positive (left) marginal wavenumber α_0 and is positive for $\alpha > \alpha_0$. Here, $m = 10$. (d) α_0 grows with m, logarithmically at large m. (In all plots, $M^{(0)} = 2$ and $n = 2$.)

We know that the (largest) growth rate of two-dimensional normal modes always increases with s (see figure 5). It follows that if at some given parameter values there are no growing two-dimensional normal modes, then there are no growing three-dimensional ones as well. (Otherwise, there would have been a growing two-dimensional mode at a smaller s, and then this mode would be growing at the given s as well, in contradiction with the assumption.) So, to determine the set of critical points (for the onset of instability) of the parameter space, it is sufficient to consider two-dimensional normal modes.

Appendix D. The limit $\sigma_0 \to 0$

Consider the limiting case $\sigma_0 \to 0$. Our non-dimensionalization (2.5) clearly breaks down at $\sigma_0 = 0$. Instead, one can choose the units of measurement based on the speed $U^{(0)} = s^* d_1$, so that $t^{(0)} = t^*/(d_1/(s^* d_1)) = s^* t^*$, where s^* is the dimensional basic shear rate at the interface. Similarly, $p^{(0)}$ and $\sigma^{(0)}$ are obtained by changing from σ_0 to $\mu_1 U^{(0)}$ in equations (2.5). The new Marangoni number is $M^{(0)} = E\Gamma_0/(\mu_1 U^{(0)}) = M/s$, where $s = s^* d_1/(\sigma_0/\mu_1)$ is interpreted as the modified capillary number, $Ca^{(0)} = \mu_1 U^{(0)}/\sigma_0$.
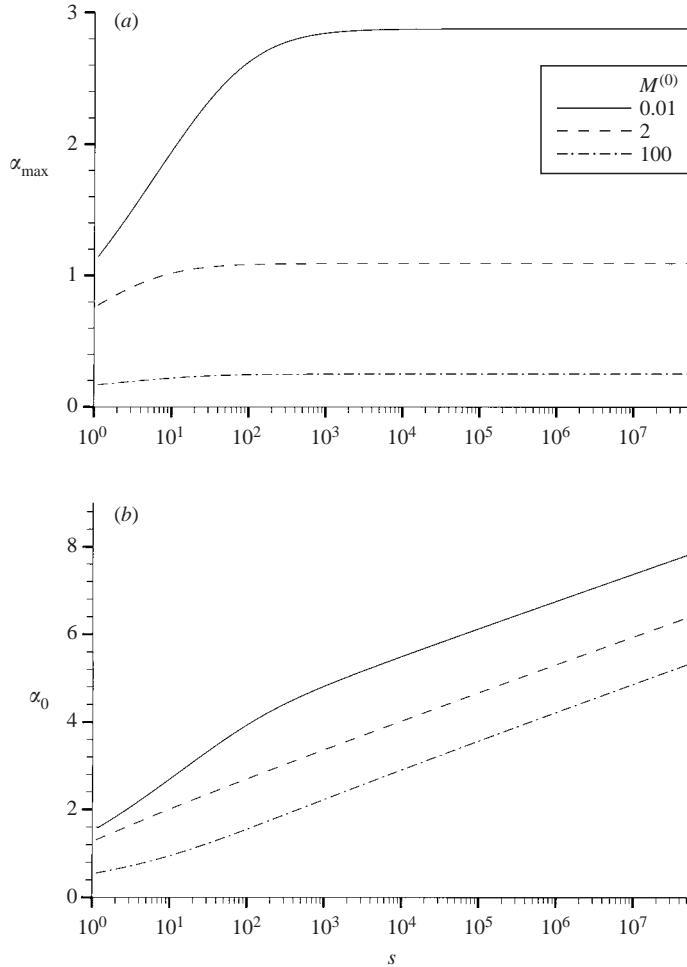
FIGURE 18. Small-σ_0 (large-s) behaviour of characteristic wavenumbers: (*a*) The instability-maximizing wavenumber $\alpha_{\max}$ remains bounded as $\sigma_0 \to 0$ and (*b*) the marginal wavenumber α_0 is a logarithmically increasing function of s. (Here, $m = 0.1$, $n = 2$.)

The modified governing equations are also obtainable formally by substituting $c = c^{(0)}s$ and $M = M^{(0)}s$ into the old ones. Then we arrive at the quadratic equation for $c^{(0)}$ of the form (3.19) with the modified coefficients $q_0^{(0)} = q_0/s^2$, $q_1^{(0)} = q_1/s$ and $q_2^{(0)} = q_2$ where the formulae (3.20)–(3.22) for q_0, q_1 and q_2 are taken with $M = M^{(0)}s$. (To prevent any misinterpretation we note that the dimensionless $s \to \infty$ here simply because the unit of measurement $\sigma_0/(\mu_1 d_1)$ of the fixed dimensional s^* approaches zero as $\sigma_0 \to 0$. The dimensional profiles $\bar{u}^* = s^*y + q^*y^{*2}$ do not change as $\sigma_0 \to 0$.) In the limit $s^{-1} = 0$ (corresponding to $\sigma_0 = 0$), it turns out that for $m < n^2$ the dispersion curve never crosses the α-axis; the growth rate only approaches zero from above as $\alpha \to \infty$ – as illustrated in figure 17(*a*) (with a sample choice of values of control parameters). We can use the modified equation (A 3), retaining only the terms which are dominant at large α,

$$-q_{1I}^{(0)3}c_I^{(0)} + q_2^{(0)}q_{0I}^{(0)2} - q_{1R}^{(0)}q_{0I}^{(0)}q_{1I}^{(0)} = 0, \qquad (D\,1)$$

with

$$q_{0I}^{(0)} = -\frac{M^{(0)}N}{2}, \quad q_{1R}^{(0)} = (1-m)N, \quad q_{1I}^{(0)} = -\frac{(m+1)M^{(0)}N\beta}{2}, \quad q_{2}^{(0)} = -(m+1)^2N\beta,$$

(D 2)

where $\beta = e^{2\alpha}/(4\alpha)$ and $N = e^{2\alpha n}/4$, to obtain the leading large-α asymptotics (the subscript 0 indicates the case $\sigma_0 = 0$):

$$\gamma_0^{(0)}(\alpha) \sim \frac{64}{M^{(0)}(m+1)^2} \frac{\alpha^3}{e^{4\alpha}},$$

(D 3)

which is exponentially small and independent of n, and so positive for all n and m. (In particular, the instability threshold $m = n^2$ for $M < 5/2$ does not exist for the case $\sigma_0 = 0$.) The numerical solutions confirm this asymptotic behaviour, as in figure 17(*b*).

The growth rate (D 3) is positive and that for $\sigma_0 \neq 0$, (4.15), is strictly negative. However, we find that the marginal-stability wavenumber α_0 is an unbounded increasing function of s, and this takes care of continuity of the growth rate function as $s^{-1} \to 0$. The asymptotic behaviour of α_0 is readily obtained from the modified equation (A 3) with $c_I = 0$ and the asymptotic expressions given by (D 2) and, in addition, $q_{0R}^{(0)} = M^{(0)}s^{-1}\beta N/4$ (keeping only the leading terms with respect to the small parameter s^{-1} in the equation):

$$\frac{e^{4\alpha_0}}{\alpha_0^2} \sim \frac{128s}{M^{(0)}(m+1)}.$$

(D 4)

This is borne out by the numerical solution of the exact quadratic equation as shown in figure 18(*b*). (Also, as an implication, the convergence of the growth rate function is non-uniform at large wavenumbers in the limit $\sigma_0 \to 0$.) In contrast, the wavenumber α_{max} maximizing the growth rate remains bounded as shown in figure 18(*a*).

The result (D 3) means instability for $m \geqslant n^2$ as well. However, we know that the long waves are stable for $m \geqslant n^2$. Thus, there should be a marginal-stability wavenumber $\alpha_0 \neq 0$, as figure 17(*c*) confirms. As figure 17(*d*) shows, $\alpha_0(m)$ is growing, logarithmically at large m, independently of M and n. Thus, in the case of $m \geqslant n^2$ at $\sigma_0 = 0$, the instability has a short-wave character, in contrast to the long-wave instability for $\sigma_0 > 0$ with $M < 5/2$ and $m < n^2$. However, it is clear that at any $\sigma_0 \neq 0$, no matter how small, sufficiently short waves are stabilized, and the instability is only a mid-wave one.

REFERENCES

ANSHUS, B. E. & ACRIVOS, A. 1967 The effect of surface active agents on the stability characteristics of falling liquid films. *Chem. Engng Sci.* **22**, 389–393.

BABCHIN, A. J., FRENKEL, A. L., LEVICH, B. G. & SIVASHINSKY, G. I. 1983*a* Flow-induced nonlinear effects in thin liquid film stability. *Ann. NY Acad. Sci.* **404**, 426–428.

BABCHIN, A. J., FRENKEL, A. L., LEVICH, B. G. & SIVASHINSKY, G. I. 1983*b* Nonlinear saturation of Rayleigh-Taylor instability in thin films. *Phys. Fluids* **26**, 3159–3161.

CARROLL, B. J. & LUCASSEN, J. 1974 Effect of surface dynamics on process of droplet formation from supported and free liquid cylinders. *J. Chem. Soc. Faraday Trans.* **70**, 1228–1239.

CASSIDY, K. J., HALPERN, D., RESSLER, B. G. & GROTBERG, J. B. 1999 Surfactant effects in model airway closure experiments. *J. Appl. Physiol.* **87**, 415–427.

CHARRU, F. & HINCH, E. J. 2000 'Phase diagram' of interfacial instabilities in a two-layer Couette flow and mechanism of the long-wave instability. *J. Fluid Mech.* **414**, 195–223.

DE WIT, A., GALLEZ, D. & CHRISTOV, C. I. 1994 Nonlinear evolution equations for thin liquid films with insoluble surfactants. *Phys. Fluids* **6**, 3256–3266.

DRAZIN, P. G. & REID, W. H. 1981 *Hydrodynamic Stability*. Cambridge University Press.

FRENKEL, A. L., BABCHIN, A. J., LEVICH, B. G., SHLANG, T. & SIVASHINSKY, G. I. 1987 Annular flow can keep unstable flow from breakup: nonlinear saturation of capillary instability. *J. Colloid Interface Sci.* **115**, 225–233.

FRENKEL, A. L. & HALPERN, D. 2002 Stokes-flow instability due to interfacial surfactant. *Phys. Fluids* **14**, L45–L48.

GUMERMAN, R. J. & HOMSY, G. M. 1974 Convective instabilities in concurrent two-phase flow: Part I. Linear stability. *AIChE J.* **20**, 981.

HALPERN, D. & FRENKEL, A. L. 2001 Saturated Rayleigh-Taylor instability of an oscillating Couette film flow. *J. Fluid Mech.* **446**, 67–93.

HALPERN, D. & GROTBERG, J. B. 1993 Surfactant effects on fluid elastic instabilities of liquid lined flexible tubes: a model of airway closure. *Trans. ASME: J. Biomech. Engng* **115**, 271–277.

HESLA, T. I., PRANCKH, F. R. & PREZIOSI, L. 1986 Squire's theorem for two stratified fluids. *Phys. Fluids* **29**, 2808–2811.

HOOPER, A. P. 1985 Long-wave instability at the interface between two viscous fluids: Thin layer effects. *Phys. Fluids* **28**, 1613–1618.

HOPF, L. 1914 Der verlauf kleiner schwingungen auf einer stromung reibender flussigkeit. *Ann. Phys. Leipzig* **44**, 1–60.

HU, H. H. & JOSEPH, D. D. 1989 Lubricated pipelining: stability of core-annular flow. Part 2. *J. Fluid Mech.* **205**, 359–396.

JOSEPH, D. D. & RENARDY, Y. 1993 *Fundamentals of Two-Fluid Dynamics, Vol I: Mathematical Theory and Applications*. Springer.

KISTLER, S. F. & SCHWEIZER, P. M. (Ed.) 1997 *Liquid Film Coating*. Chapman Hall.

KWAK, S. & POZRIKIDIS, C. 2001 Effect of surfactants on the instability of a liquid thread or annular layer. Part i: Quiescent fluids. *Intl J. Multiphase Flow* **27**, 1–37.

LI, X. & POZRIKIDIS, C. 1997 The effect of surfactants on drop deformation and on the rheology of dilute emulsions in stokes flow. *J. Fluid Mech.* **341**, 165–194.

LIN, S. P. 1970 Stabilizing effects of surface-active agents on a film flow. *AIChE J.* **16**, 375.

VON MISES, R. 1912 Kleine schwingungen und turbulenz. *Jber. Deutsch. Math.-Verein* **21**, 241–248.

OTIS, D. R., JOHNSON, M., PEDLEY, T. J. & KAMM, R. D. 1993 Role of pulmonary surfactant in airway closure: a computational study. *J. Appl. Physiol.* **75**, 1323–1333.

RUBINSTEIN, B. Y. & BANKOFF, S. G. 2001 Dynamics of thin liquid films on a coated solid surface with insoluble surfactants: weakly nonlinear analysis. *Langmuir* **17**, 1306–1307.

SLATTERY, J. C. 1974 Interfacial effects in the entrapment and displacement of residual oil. *AIChE J.* **20**, 1145–1154.

WHITAKER, S. 1964 Effect of surface active agents on the stability of falling liquid films. *Indust. Engng Chem. Fundam. Q.* **3**, 132.

WHITAKER, S. & JONES, L. O. 1966 Stability of falling liquid films. Effect of interface and interfacial mass transport. *AIChE J.* **12**, 421–431.

WONG, H., RUMSCHITZKI, D. & MALDARELLI, C. 1996 On the surfactant mass balance at a deforming fluid interface. *Phys. Fluids* **8**, 3203–3204.

YIANTSIOS, G. & HIGGINS, G. 1988 Linear stability of plane Poiseuille flow of two superposed fluids. *Phys. Fluids* **31**, 3225–3238.

YIH, C. S. 1966 Instability of laminar flows due to a film of adsorption. *J. Fluid Mech.* **28**, 493–500.

YIH, C. S. 1967 Instability due to viscosity stratification. *J. Fluid Mech.* **27**, 337–352.